$Ca_V2.1$ α_1 subunit motifs that control presynaptic $Ca_V2.1$ subtype abundance are distinct from $Ca_V2.1$ preference

Jianing Li[1,2], Priyadharishini Veeraraghavan[1], Samuel M. Young, Jr[1,3^]

[1]Department of Anatomy and Cell Biology, University of Iowa, Iowa City, IA, USA.
[2]Cell Developmental Biology Graduate Program, University of Iowa, Iowa City, IA 52242, USA
[3]Department of Otolaryngology, Iowa Neuroscience Institute, University of Iowa, Iowa City, IA, USA.

^Correspondence
Samuel M. Young, Jr. PhD
Department of Anatomy and Cell Biology
University of Iowa
PBDB 5322
169 Newton Road
Iowa City, IA 52242
Email: samuel-m-young@uiowa.edu

ORCIDs:

Jianing Li	0000-0001-5384-773X
Priyadharishini Veeraraghavan	0000-0003-2826-1686
Samuel M. Young, Jr.	0000-0002-7589-7612

Key points summary:

- Presynaptic Ca_V2 subtype abundance regulates neuronal circuit properties, however the mechanisms regulating presynaptic Ca_V2 subtype abundance and preference remains enigmatic.
- The Ca_V α_1 subunit determines subtype and contains multiple motifs implicated in regulating presynaptic subtype abundance and preference.
- The $Ca_V2.1$ α_1 subunit domain II-III loop and cytoplasmic C-terminus are positive regulators of presynaptic $Ca_V2.1$ abundance but do not regulate preference.
- The $Ca_V2.3$ α_1 subunit cytoplasmic C-terminus negatively regulates presynaptic Ca_V2 subtype abundance but not preference while the $Ca_V2.2$ α_1 subunit cytoplasmic C-terminus is not a key regulator of presynaptic Ca_V2 subtype abundance or preference.
- The Ca_V2 α_1 subunit motifs determining the presynaptic Ca_V2 preference are distinct from abundance.

Abstract

Presynaptic voltage-gated Ca^{2+} channels (Ca_V) subtype abundance at mammalian synapses regulates synaptic transmission in health and disease. In the mammalian central nervous system, most presynaptic terminals are $Ca_V2.1$ dominant with a developmental reduction in $Ca_V2.2$ and $Ca_V2.3$ levels, and Ca_V2 subtype levels are altered in various diseases. However, the molecular mechanisms controlling presynaptic Ca_V2 subtype levels are largely unsolved. Since the Ca_V2 α_1 subunit cytoplasmic regions contain varying levels of sequence conservation, these regions are proposed to control presynaptic Ca_V2 subtype preference and abundance. To investigate the potential role of these regions, we expressed chimeric $Ca_V2.1$ α_1 subunits containing swapped motifs with the $Ca_V2.2$ and $Ca_V2.3$ α_1 subunit on a $Ca_V2.1/Ca_V2.2$ null background at the calyx of Held presynaptic terminal. We found that expression of $Ca_V2.1$ α_1 subunit chimeras containing the $Ca_V2.3$ loop II-III region or cytoplasmic C-terminus (CT) resulted in a large reduction of presynaptic Ca^{2+} currents compared to the $Ca_V2.1$ α_1 subunit. However, the Ca^{2+} current sensitivity to the $Ca_V2.1$ blocker Agatoxin-IVA, was the same between the chimeras and the $Ca_V2.1$ α_1 subunit. Additionally, we found no reduction in presynaptic Ca^{2+} currents with $Ca_V2.1/2.2$ cytoplasmic CT chimeras. We conclude that the motifs in the $Ca_V2.1$ loop II-III and CT do not individually regulate $Ca_V2.1$ preference, but these motifs control $Ca_V2.1$ levels and the $Ca_V2.3$ CT contains motifs that negatively regulate presynaptic $Ca_V2.3$ levels. We propose that the motifs controlling presynaptic $Ca_V2.1$ preference are distinct from those regulating $Ca_V2.1$ levels and may act synergistically to impact pathways regulating $Ca_V2.1$ preference and abundance.

Introduction

At mammalian central nervous system (CNS) synapses, $Ca_V2.1$, $Ca_V2.2$, and $Ca_V2.3$, are key determinants of Ca^{2+} entry that controls synaptic transmission and neuronal circuit function (Dolphin & Lee, 2020; Young & Veeraraghavan, 2021). Among the three Ca_V2 subtypes, presynaptic $Ca_V2.1$ levels are dominant compared to $Ca_V2.2$ and $Ca_V2.3$ (Iwasaki & Takahashi, 1998; Iwasaki *et al.*, 2000; Nanou & Catterall, 2018; Dolphin & Lee, 2020). During neuronal circuit maturation, action-potential (AP) evoked synaptic transmission becomes increasingly $Ca_V2.1$-dependent due to a selective presynaptic reduction of $Ca_V2.2$ and $Ca_V2.3$ (Iwasaki & Takahashi, 1998; Eggermann *et al.*, 2011; Young & Veeraraghavan, 2021). In addition, presynaptic Ca_V2 subtype levels vary between synapses and are altered in various diseases (Dolphin & Lee, 2020; Young & Veeraraghavan, 2021). Since Ca_V2 subtypes differentially control Ca^{2+} influx, elucidating the molecular mechanisms controlling presynaptic Ca_V2 subtype abundance are critical to understanding brain function in health and disease.

Although presynaptic Ca_V2 subtype levels are highly variable, they are distinct between the neuronal soma and presynaptic terminal (Doughty *et al.*, 1998). In addition, loss of $Ca_V2.1$ leads to increases in presynaptic $Ca_V2.2$ levels, however total presynaptic Ca^{2+} currents are reduced (Jun *et al.*, 1999; Inchauspe *et al.*, 2004; Lubbert *et al.*, 2017). Therefore, it is proposed that mechanisms that control presynaptic Ca_V2 levels and preferences are distinct from those controlling somatic Ca_V2 levels (Weiss & Zamponi, 2017; Dolphin & Lee, 2020). However, whether the mechanisms that determine presynaptic Ca_V2 subtype preference and abundance are interrelated or separable are unknown.

The pore- forming Ca_V2 α_1 subunit determines presynaptic Ca_V2 preference and contains multiple cytoplasmic protein interaction motifs (Dolphin & Lee, 2020). Due to varying levels of sequence conservation between the three Ca_V2 α_1 subunit isoforms cytoplasmic regions, three regions are implicated in regulating presynaptic Ca_V2 channel levels. They are: 1) the I-II loop; the primary binding site to the $Ca_V\beta$ subunit (AID) 2) the II-III loop; the synprint domain; and 3)

the C-terminal region, which contains multiple active zone (AZ) protein binding sites and is frequently mutated in Ca_V2 channelopathies (Dolphin & Lee, 2020; Young & Veeraraghavan, 2021). Since the loop II-III and cytoplasmic CT regions are not highly conserved between the different Ca_V2 α_1 subunit isoforms and are subject to alternative splicing (Simms, 2014), they are speculated to contain motifs that regulate the presynaptic Ca_V2 subtypes levels and preference. However, the identity of the Ca_V2 α_1 subunit motifs that regulate presynaptic Ca_V2 subtype levels and preference is unclear. Studies from cultured superior cervical ganglion neurons demonstrated that the $Ca_V2.1$ loop II-III domain regulates presynaptic targeting (Mochida *et al.*, 2003). However, it is not defined if the $Ca_V2.1$ loop II-III region is a key determinant of preference or if the II-III region from other Ca_V2 subtypes regulates abundance and preference. Although motifs in the $Ca_V2.1$ CT (aa. 2016-2368) that interact with AZ proteins are dispensable for controlling presynaptic $Ca_V2.1$ abundance (Lubbert *et al.*, 2017), it is not known if other regions in the $Ca_V2.1$ CT control Ca_V2 subtype abundance and preference. Furthermore, whether the $Ca_V2.2$ and $Ca_V2.3$ CT regulates abundance and preference is unresolved.

To elucidate the roles of the Ca_V2 α_1 subunit loop II-III and CT in regulating presynaptic abundance and preference in a native neuronal circuit, we generated Ca_V2 α_1 subunit chimeras: 1) <u>$Ca_V2.1/2.3$ chimeras</u>, the $Ca_V2.1$ α_1 subunit II-III loop and/or CT region, were swapped with these regions from the $Ca_V2.3$ α_1 subunit. 2) <u>$Ca_V2.1/2.2$ chimeras,</u> $Ca_V2.1$ α_1 subunit CT region was swapped with the $Ca_V2.2$ α_1 subunit CT region. We then used helper-dependent Adenoviral (HdAd) technology and delivery techniques to express $Ca_V2.1$ α_1 subunit chimeras on a $Ca_V2.1/Ca_V2.2$ null background at the postnatal days (P) 9–11 calyx of Held using a *Cacna1a*/*Cacna1b flox/flox* ($Ca_V2.1$ $Ca_V2.2$ CKO) mouse model. The calyx of Held is a large glutamatergic presynaptic terminal in the auditory brainstem that at this developmental stage contains multiple Ca_V2 subtypes which is similar to the majority of presynaptic terminals (Iwasaki *et al.*, 2000; Young & Veeraraghavan, 2021).

Using direct presynaptic Ca^{2+} current recordings at the calyx of Held, we found that ablation of $Ca_V2.1$ and $Ca_V2.2$ resulted in a significant reduction in total presynaptic Ca^{2+} currents and were insensitive ω-Agatoxin-IVA (Aga), a $Ca_V2.1$ specific blocker, and ω-Conotoxin GVIA (Cono), a $Ca_V2.2$ specific blocker, and Nifedipine a Ca_V1 specific blocker, but were partially sensitive to SNX-482, a $Ca_V2.3$ specific blocker. Expression of $Ca_V2.1/2.3$ chimeras with single or combined region swaps resulted in a significant reduction in peak Ca^{2+} current amplitudes. However, the remaining Ca^{2+} currents with the single swap $Ca_V2.1/2.3$ chimeras exhibited a similar proportion of Aga sensitive currents as the full transcript (FT) $Ca_V2.1$ α_1 subunit, while the combined swap had a significant increase in Aga insensitive Ca^{2+} currents. In addition, expression of $Ca_V2.1/2.3$ chimeras which replaced the dispensable region of the $Ca_V2.1$ CT (aa. 2016-2368) with corresponding $Ca_V2.3$ CT region resulted in a reduction in Ca^{2+} currents. Finally, we found that expression of $Ca_V2.1/2.2$ CT chimeras revealed no reduction in presynaptic Ca^{2+} currents.

Based on our data, we conclude that individual motifs in the $Ca_V2.1$ α_1 subunit loop II-III or CT are positive regulators of presynaptic $Ca_V2.1$ levels but do not individually control $Ca_V2.1$ preference. Furthermore, we conclude the $Ca_V2.3$ CT contains motifs that negatively regulate presynaptic $Ca_V2.3$ levels. Therefore, we propose that the motifs that determine presynaptic $Ca_V2.1$ abundance are distinct from those regulating $Ca_V2.1$ preference and these motifs may synergistically impact pathways that regulate $Ca_V2.1$ preference and levels.

Methods and materials

Ethical approval

All procedures were performed according to the animal welfare law of the University of Iowa Office of Animal Resources (OAR) and Institutional Animals Care and Use Committee (IACUC, D16-00009 (A3021-01)). Mice are maintained at The University of Iowa Animal Care Facility which is approved under NIH assurance A3021-01 and certified by the State of Iowa for use of living animals. Animals were housed with 12 h light/dark cycle and *ab libitum* food/water supply. Animals of both sexes at postnatal day 9-11 were used for all experiments. All available measures were taken to minimize animal pain and suffering.

EXPERIMENTAL DESIGN

Generation of *Cacna1a*/*Cacna1b* flox/flox animal

Cacna1a fl/fl mice

Cacna1a$^{fl/fl}$ mice were generated as follows. The Cacna1a$^{tm1a(EUCOMM)Hmgu}$ targeting vector (EUMMCR) was electroporated into the JM8A3 ES-cells derived from C57BL/6N mice and clones were selected and PCR verified. The neo gene was removed by crossing to FLPo mice carrying the FLP recombinase gene under the control of the CAG promoter (C57BL/6N-Tg (CAG-Flpo)1Afst/Mmucd, stock 036512-UCD. (Mouse Biology Program KOMP). Genotyping of *Cacna1a* flox mice by PCR was carried out by the following primers,

754 5' GGAATCCCAAGTGCGTGAGTCTCC 3'

887 5' TCAGCCCCTTCTCTTTAATCTGACCC 3'

Cacna1a$^{fl/fl}$ mice were backcrossed to C57BL6/J background.

Cacna1b$^{fl/fl}$ *mice*

Cacna1b$^{fl/fl}$ *mice* (*C*57BL/6N-Cacna1b$^{tm1c(KOMP)Wtsi}$/H) were purchased from MRC Harwell Institute. Genotyping of *Cacna1b*$^{fl/fl}$ was carried out using the following primers,

Cacna1b-5arm-WTF 5' TTGGTGTCCTGTTCTCCACA 3'

Cacna1b-Crit-WTR 5' CAGGGAATCCTGGGAAGTAA 3'

5mut-R1 5' GAACTTCGGAATAGGAACTTCG 3'

Cacna1b$^{fl/fl}$ *mice* were backcrossed to the C57BL6/J background.

Cacna1a$^{fl/fl}$*, Cacna1b*$^{fl/fl}$ mice

Cacna1a$^{fl/fl}$*, Cacna1b*$^{fl/fl}$ mice were generated by crossbreeding *Cacna1a*$^{fl/fl}$ with *Cacna1b*$^{fl/fl}$ to homozygosity. Genotyping was performed by PCR.

Stereotactic P1 surgery

Stereotactic surgery was performed at P1 as described previously (Radulovic *et al.*, 2020). Briefly, *Cacna1a*$^{fl/fl}$, *Cacna1b*$^{fl/fl}$ mice were anesthetized by hypothermia, using ice bath for 5min. Subsequently, ~2 µl HdAd in storage buffer (in Mm: 10 HEPES, 250 sucrose, 1 $MgCl_2$ at pH: 7.4 and 6.6% mannitol) was injected at 1 µl/min into the cochlear nucleus (CN) using pulled glass pipettes with a 20 µm opening (Sutter Instrument, P-97, U.S.A.). Two viral vectors, expressing Cre and Ca_V2 α_1 hybrid constructs were co-injected. The total viral particle delivered did not exceed $2*10^9$ viral particles. To dissipate pressure after injection, the needle was slowly removed. Animals were then placed under a warming lamp. Upon full recovery, visual inspection and tail pinch responsiveness, animals were returned to their respective cage with the dam. If animals did not recover from the surgery, they were immediately euthanized. In the case of runting or if animals were found in distress at later time points the veterinary staff was consulted and their recommendation for further action was followed.

DNA constructs and recombinant viral vector production

$Ca_V2.1$ chimeras

Codon optimized (GENEart) $Ca_V2.1$ α_1 subunit cDNA Cacna1a (*Mus musculus*, Accession No. NP_031604.3), $Ca_V2.2$ α_1 subunit cDNA Cacna1b (*Mus musculus,* Accession No. NP_001035993.1) and $Ca_V2.3$ α_1 subunit cDNA Cacna1e (*Mus musculus*, Accession No. NP_033912.2) were used to generate Ca_V2 α_1 hybrid constructs. All Ca_V2 hybrid constructs were sequenced verified. Amino acid alignment of above constructs were performed under

Clustal Omega function using the MegAlign Pro 17 program implemented in the Lasergene software package (v.17, DNASTAR). The following Ca_V2 hybrid constructs were created.

<u>$Ca_V2.1/2.3$ II-III loop</u>: $Ca_V2.1$ α_1 subunit aa. 719-1210 replaced with $Ca_V2.3$ α_1 subunit aa. 707-1151

<u>$Ca_V2.1/2.3$ CT</u>: $Ca_V2.1$ α_1 subunit aa. 1933-2368 replaced with $Ca_V2.3$ α_1 subunit aa. 1897-2273

<u>$Ca_V2.1/2.3$ II-III loop CT</u>: $Ca_V2.1$ α_1 subunit aa. 719-1210 replaced with $Ca_V2.3$ α_1 subunit aa. 707-1151 and $Ca_V2.1$ α_1 subunit aa. 1933-2368 replaced with $Ca_V2.3$ α_1 subunit aa. 1897-2273

<u>$Ca_V2.1/2.2$ CT</u>: $Ca_V2.1$ α_1 subunit aa. 1933-2368 replaced by $Ca_V2.2$ α_1 subunit aa. 1870-2327

<u>$Ca_V2.1/2.3$ CT1</u>: $Ca_V2.1$ α_1 subunit aa. 2016-2368 replaced with $Ca_V2.3$ α_1 subunit 1952-2273

<u>$Ca_V2.1/2.3$ CT2</u>: $Ca_V2.1$ α_1 subunit aa. 1967-2368 replaced by $Ca_V2.3$ α_1 subunit 1929-2273

For presynaptic Ca^{2+} currents recordings in acute brain slices, these constructs were individually cloned into the EcoRI and NotI sites of the 470 bp human synapsin (hSyn) neurospecific expression cassette (Montesinos *et al.*, 2016; Dong *et al.*, 2018). For Ca^{2+} currents recordings in HEK293T cells, these constructs were individually cloned into the EcoRI and NotI sites of the 463bp human CMV promoter expression cassette (Tarabichi *et al.*, 2023).

HdAd production

Helper-dependent Adenoviral vector (HdAd) (Cre) which co-expresses Cre recombinase (Cre and EGFP or mCherry under separate neurospecific expression cassettes driven by the 470 bp human synapsin promoter (hSyn) was produced as previously described (Montesinos *et al.*, 2016; Dong *et al.*, 2018). To produce HdAd Ca_V2 chimeric viruses we followed standard protocols (Montesinos *et al.*, 2016; Lubbert *et al.*, 2017). Briefly, Ca_V2 α_1 chimera cDNA constructs driven by hSyn promoter expression cassette or a high-level overexpression pUNISHER (Pun) cassette were then cloned into the AscI site, pdelta23E4 which contains a separate neuro-specific expression of mCherry or myristolated EGFP (mEGFP) markers (Montesinos *et al.*, 2011). Production of HdAd was carried out as previously described (Palmer & Ng, 2005; Montesinos *et al.*, 2016). The HdAd plasmid was linearized with PmeI and then

transfected (Profection Mammalian Transfection System, Promega, Madison, WI, USA) into 116 producer cells. Helper virus (HV) was added the following day. Forty-eight hours post infection, cells were subjected to three freeze/thaw cycles and lysate was collected. The HdAd vectors were amplified for total of five serial coinfections from 3x6 cm tissue culture dishes followed by one 15 cm dish and finally 30x15 cm dishes of 116 cells (confluence ~90%). HdAd was purified by CsCl ultracentrifugation. HdAd was stored at -80°C in storage buffer (10 mM Hepes, 1 mM $MgCl_2$, 250 mM Sucrose, pH 7.4).

HdAd titering and quality control

HdAds were titered by qPCR as described previously (Lubbert *et al.*, 2019a). The purified reference virus (RV); Ad5-CMV-EGFP (UNC, Gene Therapy Center, Chapel Hill, North Carolina) was titered by endpoint dilution and by transducing units, as described previously (Bewig & Schmidt, 2000). Human Adenovirus 5 Reference Material (ARM), (ATCC, VR-1516). To titer the HdAd by qPCR, adenoviral gDNA from HdAd, RV and ARM was purified from 6 cm plates. Plates were seeded with 3.75 x 10^6 HEK293 cells in DMEM with 10% FBS and coinfected with HdAd plus RV on the following day at a multiplicity of 100 vp/cell. The cells were incubated for 1 hr at 37°C with 5% CO_2 and washed to remove unabsorbed virions. Cells were harvested 4 hr post-infection, then washed with 1 mL PBS and centrifuged for 5 min at 4°C. Pellets were resuspended in 100 mM Tris-HCl, pH 8, lysed by freeze/thaw cycles and treated with 20 U/mL Benzonase for 10 min. Subsequently, lysate was incubated in Proteinase K-SDS solution for 3 hr at 50°C. After protein precipitation with 1.65 M NaCl on ice, DNA was precipitated from supernatants with isopropanol and 3 M sodium acetate, pH 5.2. Samples were mixed well and incubated for 1 hr at -80°C then spun at 4°C for 30 min. Pellets were washed with cold ethanol, dried and resuspended in 10 mM Tris-Cl, pH 8.0. A plasmid standard containing three specific DNA sequences; Ad5 E1a (replication-competent Adenovirus (RCA) detection), Ad5 E2B Iva2 (viral DNA polymerase and terminal protein precursor, HV-exclusive), and Ad genomic stuffer sequence (Cosmid 346 and HPRT1 gene, in all HdAd-exclusive) was

used. Three specific primer/probe sets were used for these 3 regions in the plasmid for the detection in qPCR:

1.) **Ad5 E1a (RCA):** probe: NED-5'-AGCACCCCGGGCACGGTTG-3'-MGBNFQ; fwd: 5'-GGGTGAGGAGTTTGTGTTAGATTATG-3'; rev: 5'-TCCTCCGGTGATAATGACAAGA-3'
2.) **E2B Iva2 (HV):** probe: FAM-5'-TGTCTTTCAGTAGCAAGCT-3'-TAMRA, HV fwd primer: 5'-TGGGCGTGGTGCCTAAAA-3', rev: 5'-GCCTGCCCCTGGCAAT-3'
3.) **Genomic stuffer DNA (HdAd):** probe: VIC-5'- AGCCTCTCTCATCTCACAGT -3'-MGBNFQ, fwd: 5'-CCCCGCTACCCCAATCC-3', rev: 5'-TTAGCTTTTTTGGGTGATTTTTCC-3'.

Sample DNA was diluted 1:10^3, 1:10^4 or 10^5 in 10 mM Tris-Cl, pH 8.0. For HdAd and HV probes, a 6-point standard curve was constructed with the plasmid standard using 10^7- 10^2 molecules/well. For RCA detection, two 7-point curves were constructed with 10^7 - 10 molecules/well (one plasmid standard and one using ARM gDNA spiked with 10^7 copies of HdAd gDNA). Real-Time PCR parameters were 50°C for 2 min, 95°C for 10 min; 40 cycles of: 95°C for 15 sec, 60°C for 1 min. Outliers and results out of range of standard curve were discarded. Results within range of the standard curve were corrected for their dilution and determined as HdAd vector genomes/mL. All samples were negative for RCA.

To determine the IU copies/mL from purified coinfection samples, averaged results were divided by 3 µL and multiplied by 25 µL giving IU copies/coinfection. Next, this number was divided by the volume in µL of HdAd added to the coinfection giving IU copies/µL then multiplied by 1000 to obtain the i,nfectious HdAd genomes/mL.

Calculation to determine the titer of purified HdAd virus:

$$HdAd\ infectivity = RV\ infectivity * \frac{HdAd\ vector\ genomes/RV\ genomes}{infectious\ HdAd\ genomes/infectious\ RV\ genomes}$$

where Ad5-CMV-EGFP is RV, RV infectivity is VP/IU. IU is the average titer of end point dilution and transducing unit assays, HdAd vector genomes and RV genomes are the number of

genomes from purified virus as determined by qPCR, and infectious HdAd genomes and infectious RV genomes are the number of genomes in DNA purified from coinfections. The titers of HdAds carry different cDNA constructs are listed as follow, viral particle/ml: Cre EGFP, $1.75*10^{12}$, Cre mCherry, $2.41*10^{12}$, syn $Ca_V2.1$ FT, $2.40*10^{12}$, Pun $Ca_V2.1$ FT, $2.19*10^{12}$, $Ca_V2.1/2.3$ II-III loop CT, $2.00*10^{12}$, $Ca_V2.1/2.3$ II-III loop, $2.07*10^{12}$, Syn $Ca_V2.1/2.3$ CT, $1.90*10^{12}$, Pun $Ca_V2.1/2.3$ CT, $3.11*10^{12}$, $Ca_V2.1$ delta 2016, $1.40*10^{12}$, $Ca_V2.1/2.3$ CT 2016-2368, $4.70*10^{12}$, $Ca_V2.1/2.3$ CT 1967-2368, $3.29*10^{12}$, syn $Ca_V2.1/2.2$ CT, $3.17*10^{12}$, Pun $Ca_V2.1/2.2$ CT, $9.52*10^{12}$. Particle to infectious unit ratio was 10:1~ 50:1. Either syn Cre syn EGFP or syn Cre syn mCherry was used to make sure that the viruses expressing Cre carry different fluorescent protein than the viruses expressing Ca_V2 constructs.

Western Blot

To determine expression of our $Ca_V2.1$ chimeric constructs, we performed Western Blot analysis on HEK293 cells transduced with our HdAd vectors expressing the Ca_V2 α_1 chimeric constructs. To do so, HEK293 cells were infected with our HdAd vectors, and 48 hrs later cells were collected and lysed in RIPA buffer containing: 10 mM Tris-Cl pH8.0, 1mM EDTA, 1% Triton-X, 0.1% sodium deoxycholate, 0.1% SDS, 140 mM NaCl, protease inhibitor (11836153001, Roche). 20 µg of protein lysate were loaded and analyzed by SDS-PAGE followed by immunoblotting: $Ca_V2.1$ α_1 CT antibody (Synaptic Systems, #152 203, rabbit polyclonal) diluted 1:1000 (final concentration 2 µg/ml) and $Ca_V2.1$ α_1 II-III loop antibody (Alomone Labs, ACC-001, rabbit polyclonal) diluted 1:500 (final concentration 1.7 µg/ml) were incubated overnight at 4°C to blot the expression of $Ca_V2.1/2.3$ II-III loop hybrid construct, $Ca_V2.3$ α_1 CT antibody (Synaptic Systems, #152 411, mouse monoclonal) diluted 1:500 (final concentration 2 µg/ml) was incubated overnight at 4°C to blot the expression of $Ca_V2.1/2.3$ II-III loop CT and $Ca_V2.1/2.3$ CT chimeras, $Ca_V2.2$ CT antibody (Synaptic Systems, #152 311, mouse monoclonal) diluted 1:1000 (final concentration 2 µg/ml) was incubated overnight at 4°C to detect the expression of $Ca_V2.1/2.2$ CT chimera. β-actin antibody (sigma, A2228, mouse

monoclonal) diluted 1:5000 (final concentration 0.4 μg /ml) was incubated overnight at 4°C used to blot the expression of β-actin. Goat anti mouse IgG (H+L) poly-HRP (Thermo Fisher, #32230) diluted 1:2000 (final concentration 0.25 μg /ml) and goat anti rabbit IgG (H+L) poly-HRP (Thermo Fisher, #32260) secondary antibody diluted 1:2000 (final concentration 0.25 ng/ml) was incubated at room temperature for 1 hour. Protein bands were detected by chemiluminescence using ECL Western blot detection reagents (Bio-Rad, #170-5060).

Preparation of acute slices

Acute brain slices were prepared as previously described (Chen *et al.*, 2013). Briefly, after decapitation of P9-11 mice of either sex, the brains were immersed in ice-cold low Ca^{2+} artificial cerebrospinal fluid (aCSF) containing (in mM): 125 NaCl, 2.5 KCl, 3 $MgCl_2$, 0.1 $CaCl_2$, 10 glucose, 25 $NaHCO_3$, 1.25 Na_2HPO_4, 0.4 L-ascorbic acid, 3 myo-inositol, and 2 Na-pyruvate, pH 7.3-7.4 (310 mosmol/l). aCSF solution was continuously bubbled with 95% O_2 and 5% CO_2. Acute brain slices (200 μm thickness) containing MNTB were obtained using a vibrating tissue slicer (Campden 7000 smz-2, Campden Instruments LTD, Loughborough, England). Slices were immediately transferred to standard aCSF (37°C, continuously bubbled with 95% O_2-5% CO_2) containing the same chemicals as the slicing buffer except that it contained 1mM $MgCl_2$ and 1 mM $CaCl_2$. After 1 hour incubation for recovery, slices were transferred to a recording chamber with the same aCSF at room temperature (RT: 25°C).

Acute slice electrophysiology

In all experiments, slices were continuously perfused with aCSF and visualized by upright microscope (BX51W, Olympus) through 4X air or 60X water-immersion objective (LUMPlanFL N, Olympus, Tokyo, Japan) and a CCD camera (QI-Click, QImaging, Surrey, BC, Canada). Patch clamp recordings were performed by using an EPC 10/2 patch-clamp amplifier (HEKA, Lambrecht, Germany), operated by PatchMaster version 2x90.5 (Harvard Instruments, Holliston, MA, USA). Data were low-pass filtered at 6 kHz and sampled with a rate of 50 kHz. Calyces transduced with HdAd $Ca_V2.1$ α_1 chimeric constructs were identified visually with two

co-expressed mEGFP and mCherry markers. To visualize mEGFP and mCherry with light of 470 nm or 560 nm, respectively, a Polychrome V xenon bulb monochromator or a lumen Metal arc lamp was used (TILL Photonics, Grafelfing, Germany).

Presynaptic Ca^{2+} current recordings

To isolate presynaptic Ca^{2+} currents, aCSF was supplemented with 1 or 1.5 µM tetrodotoxin (TTX, Alomone labs), 100 µM 4-aminopyridin (4-AP, Tocris) and 20 mM tetraethylammonium chloride (TEA, Sigma Aldrich) to block Na^+ and K^+ channels. Calyces were whole-cell voltage clamped at -80 mV. Current-voltage (IV) relationships were recorded in the presence of 1 mM $CaCl_2$ and 1 mM $MgCl_2$ with 1.5 µM TTX while pharmacological isolation of Ca_V2 subtype components was performed in 2 mM $CaCl_2$ and 1 mM $MgCl_2$ with 1 µM TTX. To characterize the in the presynaptic terminal, we used 200 nM ω-agatoxin IVA (Alomone labs) for selective inhibition of $Ca_V2.1$ channels, 2 µM ω-conotoxin GIVA (Alomone labs) for selective inhibition of $Ca_V2.2$ channels, 200 nM SNX-482 (Alomone labs) for selective inhibition of $Ca_V2.3$ channels, 10 µM Nifedipine (Alomone labs) for selective inhibition of Ca_V1 chnannels and supplemented 0.1 mg/mL cytochrome C to prevent toxin absorption. 50µM $CdCl_2$ was used for non-selective inhibition of all VGCCs. Presynaptic patch pipette with open tip diameters 4-6 MΩ resistance were pulled from 1.5 mm thin-walled borosilicate glass (Harvard apparatus) and were filled with following internal solution (in mM): 145 Cs-gluconate, 20 TEA-Cl, 10 HEPES, 2 Na_2-phosphocreatine, 4 MgATP, 0.3 NaGTP, and 0.075 EGTA, pH 7.2, 325-340 mOsm. Pipettes were coated with dental wax to minimize stray capacitance and improve voltage clamp quality. Presynaptic series resistance was less than 15 MΩ and was compensated online to 3 MΩ or less for IV recordings or compensated to 6 MΩ for Ca_V2 subtype characterization experiments with a time lag of 10 µs by the HEKA amplifier. Leak and capacitive currents were subtracted online with a P/5 routine. Cells with series resistance >15 MΩ and leak currents > 100 pA were excluded from the analysis.

HEK 293T Cell Culture

Low-passage-number Human embryonic kidney cells transformed with SV40 T-antigen (HEK293T) cells were cultured in DMEM (Thermo Fisher Scientific) with 10% fetal bovine serum at 37°C in a humidified atmosphere with 5% CO_2. Cells were grown to 70–80% confluence and transiently transfected with 5µg CMV $Ca_V2.1/2.3$ chimera constructs, 10µg CMV $Ca_V\beta4a$ (Takahashi *et al.*, 2004) and 0.25µg CMV mClover to serve as reporter of positive transfection, following manufacturer's protocols of PolyJet reagent (SignaGen Laboratories).

HEK293T cells recordings

24-48hrs post transfection, cells were seeded in multiple 35mm dishes. 5-12 hrs post seeding, HEK293T cells were subjected to whole-cell patch clamp recordings (Gandini *et al.*, 2014b) The external solution contained the following (mM): 150 Tris, 1 $MgCl_2$, and 10 $CaCl_2$(Wang *et al.*, 2017a). The internal solution was the same as presynaptic Ca^{2+} recording internal solution, but with 5mM EGTA. Patch pipette resistances were ~3 MΩ and series resistance were compensated 80%~90% to ~1MΩ(Gandini *et al.*, 2014a). The holding potential was -80mV, and cells were depolarized to reverse potential 46-52mV with 2mV steps to identify the reversal potential, 10ms duration to ensure maximal activation.

Analysis of electrophysiological data

All data was analyzed by NeuroMatic (Rothman & Silver, 2018) in Igor Pro (version 8.0, Wavemetrics, Portland, OR, USA). Voltage dependence of channel activation was described by both peak and tail currents as functions of voltage. Peak currents were fitted according to a Hodgkin-Huxley formalism with four independent gates assuming a Goldman-Hodgkin-Katz (GHK) open-channel conductance T: with E_{rev} as reversal potential, V_m as half-maximal activation voltage per gate, and k_m as the voltage dependence of activation. Tail currents were measured as peaks minus baseline and fitted with a Boltzmann function:

$$I(V) = \mathrm{T}\frac{1-e^{-\frac{V-E_{rev}}{25mV}}}{1-e^{-\frac{V}{25mV}}}\left(1-e^{\frac{V-Vm}{Km}}\right)^{-4}$$

where $V_{1/2}$ represents the half-maximal voltage and k the corresponding slope factor.

For calculation of Q_{max}, maximal gating charge of our chimeric constructs in HEK293T cells, we measured as the time integral of the gating currents at reversal potential (Wei *et al.*, 1994; Takahashi *et al.*, 2004; Wang *et al.*, 2017b). The relative *Po* was determined by linear regression, we calculated the relative *Po* by plotting the peak tail current vs. $Q_{max.}$ (Wei *et al.*, 1994; Takahashi *et al.*, 2004; Wang *et al.*, 2017b).

Statistical analysis

All statistical tests were conducted in Prism 6 (GraphPad Software). Sample sizes for all experiments were chosen based on assuming a population with a normal distribution sample size of seven is sufficient to invoke the Central Limit Theorem. All data were tested for normal distribution by performing a Shapiro-Wilk test for normality and variances of all data were estimated and compared using Bartlett's test. Electrophysiological data were compared with one-way analysis of variance (ANOVA) with a post hoc Dunnett's test, $Ca_V2.1$ FT dataset was used as control group. In Figures and Table, data are reported as mean ± SD. Statistical significance was accepted at *$p<0.05$; **$p<0.01$; ***$p<0.001$; ****$p<0.0001$.

Results

$Ca_V2.1$ and $Ca_V2.2$ channels can be ablated at the calyx of Held in $Ca_V2.1/Ca_V2.2$ CKO mouse model.

Since ablation of $Ca_V2.1$ channels results in partial compensation of Ca_V2 current levels by $Ca_V2.2$ channels at the calyx of Held (Inchauspe *et al.*, 2004; Lubbert *et al.*, 2017), we created a $Ca_V2.1$/ $Ca_V2.2$ CKO mouse model (Fig. 1A) to allow for spatial and temporal ablation of $Ca_V2.1$ and $Ca_V2.2$ channels. To determine how presynaptic loss of $Ca_V2.1$ and $Ca_V2.2$ channels impacted presynaptic Ca_V2 currents at the calyx of Held, we injected HdAd Cre at P1 into the cochlear nucleus (CN) of $Ca_V2.1$/ $Ca_V2.2$ CKO mice to create a $Ca_V2.1^{-/-}$/ $Ca_V2.2^{-/-}$ calyx of Held. Subsequently we performed whole-cell patch clamp recordings at the P9-11 calyx of Held and characterized the total Ca^{2+} current and current sensitivity to Ca_V2 subtype-specific blockers: ω-Agatoxin IVA (Aga), $Ca_V2.1$-specific, ω-Conotoxin GIVA (Cono), $Ca_V2.2$-specific, and Cadmium (Cd^{2+}) a non-specific blocker of Ca_V currents (Fig. 1D-F, Table 1). Since sequential application of blockers takes ~10-15 minutes for complete characterization of Ca_V2 currents, we measured presynaptic Ca^{2+} current rundown at wild-type calyces in the absence of blockers after ~10-15 minutes (Fig. 1B, C). We found a ~20-70 pA (2-5%) reduction of presynaptic Ca^{2+} currents (Fig. 1J, Table 1, n=3). Subsequently, analysis of Ca^{2+} currents at the $Ca_V2.1^{-/-}$/ $Ca_V2.2^{-/-}$ calyx revealed a significant reduction (wt vs. CKO (pA): -1078 ± 260.9 (n=10) vs. -425.5 ± 219.5 (n=11), $p<0.0001$) (Fig. 1E, Table 2). We found an almost complete loss of Aga sensitive currents, 809 ± 255.6 (n=4) vs 99.22 ± 53.64 (n=5), p=0.0005; and Cono sensitive currents, 92 ± 142.2 (n=4) vs 50.8 ± 43.1 (n=5), p=0.5532). (Fig1. D and F, Table 1). Therefore, these results demonstrate successful ablation of $Ca_V2.1$ and $Ca_V2.2$ channels.

In the absence of $Ca_V2.1$ and $Ca_V2.2$, a significant Aga and Cono insensitive presynaptic Ca^{2+} current was present. Since $Ca_V2.3$ subtypes can compensate for the loss of $Ca_V2.1$ channels (Kaja *et al.*, 2006) and Ca_V1 channels can be found in some presynaptic terminals (Giugovaz-Tropper *et al.*, 2011; Young & Veeraraghavan, 2021), it was important to determine if

the combined loss of $Ca_V2.1$ and $Ca_V2.2$ resulted in compensation by $Ca_V2.3$ or Ca_V1 channels. Therefore, we characterized the sensitivity of presynaptic Ca^{2+} current to $Ca_V2.3$ and Ca_V1 specific blockers in the $Ca_V2.1^{-/-}$/ $Ca_V2.2^{-/-}$ calyx of Held. First, we used SNX-482, a $Ca_V2.3$ selective blocker and found a range of ~10% to 35% block of presynaptic Ca^{2+} currents (SNX-482 sensitive fraction 24.33 ± 9.074 %) (n=3) (Fig. 1G, H, Table 1). Since there were variable levels of Ca^{2+} current reduction with SNX-482, this indicated the remaining Ca^{2+} currents in the absence of $Ca_V2.1$ and $Ca_V2.2$ could be mediated by a combination of $Ca_V2.3$ variants that are SNX-482 sensitive and SNX-482 insensitive and/or presynaptic Ca_V1 channels. To determine if Ca_V1 channels were present, we used nifedipine, a Ca_V1 selective blocker (Fig. 1I, J) and found presynaptic Ca^{2+} currents were nifedipine insensitive as there was no difference compared to the reduced fraction of Ca^{2+} current due to rundown (Fig. 1I, J, Table 1). Therefore, we conclude that in the absence of $Ca_V2.1$ and $Ca_V2.2$ channels the compensatory presynaptic Ca^{2+} currents are mediated by mix of SNX-482 sensitive and insensitive $Ca_V2.3$ channels.

The $Ca_V2.1$ α_1 subunit loop II-III domain, and CT are positive regulators of presynaptic $Ca_V2.1$ abundance

The amino acid conservation of $Ca_V2.1$ α_1 subunit and $Ca_V2.3$ α_1 subunit loop II-III region is 33.2% and CT region from aa. 1933 onwards is 39.8%, while the loop I-II is 87.3% conserved (Figure 2A, MegAlign Pro 17, Clustal Omega). In fact, the $Ca_V2.3$ α_1 subunit loop II-III lacks a syntaxin I binding site in the synprint region although is modulated by syntaxin IA (Wiser *et al.*, 2002) but see (Pereverzev *et al.*, 2002), while the $Ca_V2.3$ α_1 subunit CT lacks many of proposed AZ protein binding motifs found in the $Ca_V2.1$ CT (Dolphin & Lee, 2020). Since the loop II-III and CT regions are the most divergent, we created $Ca_V2.1$/$Ca_V2.3$ α_1 subunit chimeras that swapped the loop II-III and CT domains to determine if these domains regulated presynaptic $Ca_V2.1$ abundance and preference (Fig. 2B). We generated three HdAd $Ca_V2.1$/2.3 α_1 subunit chimeric constructs (Figure 2C). There were <u>$Ca_V2.1$/2.3 II-III loop</u>, which contains the $Ca_V2.3$ α_1 subunit loop II-III domain (aa. 707 to aa. 1151), <u>$Ca_V2.1$/2.3 CT</u>, which contains the cytoplasmic

$Ca_V2.3$ CT (aa. 1897 to aa. 2273), and $Ca_V2.1/2.3$ II-III+CT which contains both the $Ca_V2.3$ α_1 subunit loop II-III and CT (Fig. 3C). To validate that the chimeras were expressed as full-length proteins, we performed Western Blot analysis of HEK293 cells infected with our HdAd $Ca_V2.1/2.3$ chimeric constructs. Based on our results, we found that all constructs were successfully expressed (Figure 2D-F). Rescue experiments with an HdAd vector that expressed the $Ca_V2.1$ α_1 subunit FT (Mus musculus NP_031604.3) (HdAd $Ca_V2.1$ FT) in the $Cav2.1^{-/-}$ calyx of Held in a *Cacna1a* CKO mouse model has been validated to restore $Ca_V2.1$ current amplitudes, subtype levels and synaptic vesicle release rates to similar levels as wild-type calyces (Lubbert *et al.*, 2017). To validate our experimental approach, we used expressed the $Ca_V2.1$ α_1 subunit FT using HdAd $Ca_V2.1$ FT on the $Ca_V2.1$, $Ca_V2.2$ CKO mouse line. Our rescue experiments show that HdAd expression of the $Ca_V2.1$ FT in the $Ca_V2.1^{-/-}$/ $Ca_V2.2^{-/-}$ calyx of Held led to similar maximum Ca^{2+} current amplitudes and voltage-dependent activation as the wild-type calyx of Held. These results validated our experimental approach and confirming previous findings (Figure. 3, Table 2).

Subsequently, we expressed the $Ca_V2.1/2.3$ chimeras and performed direct presynaptic Ca^{2+} recordings. All chimera constructs were compared to $Ca_V2.1$ α_1 subunit FT and $Ca_V2.1^{-/-}$/ $Ca_V2.2^{-/-}$ calyces to determine rescue efficiency (Fig. 3). Since we did not find any differences in the calyx of Held size with expression of the Ca_V2 chimeras (Table 3), we reported data as maximal Ca^{2+} currents amplitude at all voltages. Current to voltage (IV) analysis revealed significant reduction in peak Ca^{2+} current amplitudes with all three chimeras compared to $Ca_V2.1$ FT (Fig. 3) However, only expression of the $Ca_V2.1/2.3$ loop II-III led to maximum Ca^{2+} currents that were larger than that of the $Ca_V2.1^{-/-}$/ $Ca_V2.2^{-/-}$ (Maximum Ca^{2+} current amplitudes (pA) $Ca_V2.1^{-/-}$/ $Cav2.2^{-/-}$: -425.5 ± 219.5 (n=11) vs. $Ca_V2.1/2.3$ II-III loop: -958.1 ± 331.3 (n=11), $p<0.0001$) (Fig. 3E).

Although we have demonstrated that changes in presynaptic Ca^{2+} currents correlate with changes in channel numbers (Lubbert *et al.*, 2017; Dong *et al.*, 2018; Lubbert *et al.*, 2019a), and

presynaptic $Ca_V2.3$ levels are significantly less than $Ca_V2.1$ and correspond to limited contribution of $Ca_V2.3$ channels to the presynaptic Ca_V2 current subtype contribution (Wu *et al.*, 1999) it was possible that the reduction in presynaptic currents with the chimeric constructs could be due to changes in the channel open probability (Po) or general mechanisms that regulate Ca_V2 channel numbers in the membrane that is not specific to regulation of presynaptic abundance. To rule out these possibilities, we expressed our $Ca_V2.1/2.3$ chimeras in HEK293T cells and measured the gating current (I_{gating}) and peak tail current (I_{tail}) at the reversal potential for Ca_V2 channels (Fig 4). The time integral of I_{gating} (Q_{max}) is an estimate of channel number (N). Analysis of Q_{max} found no difference between the chimeras, indicating that there was no change in N between the chimeras. Subsequently we plotted peak I_{tail} vs Q_{max} and performed linear regression for the constructs to determine the index of the relative Po for each construct (Fig 4). Results of our analysis revealed comparable slopes between linear regressions of the individual constructs indicating that the relative Po of the $Ca_V2.1/2.3$ chimeric channels was similar.

Based on these results, we demonstrate that $Ca_V2.1$ loop II-III and $Ca_V2.1$ CT are positive regulators of presynaptic $Ca_V2.1$ abundance but differentially regulate presynaptic $Ca_V2.1$ abundance.

The $Ca_V2.1$ α_1 subunit loop II-III and $Ca_V2.1$ α_1 subunit CT do not independently control $Ca_V2.1$ preference

Ablation of Ca_V2 subtypes leads to increased presynaptic levels of other Ca_V2 subtypes (Inchauspe *et al.*, 2004; Lubbert *et al.*, 2017) (Fig 1D, F), and overexpression of $Ca_V2.1$ results in increased presynaptic $Ca_V2.1$ levels and competes away $Ca_V2.2$, but not vice versa (Lubbert *et al.*, 2019a). Therefore, it is postulated that presynaptic Ca_V2 abundance is correlated to Ca_V2 subtype preference. Although we found a reduction of presynaptic Ca^{2+} current with the $Ca_V2.1/2.3$ chimeras, whether these regions regulated $Ca_V2.1$ preference or just abundance is unknown. Therefore, it was important to elucidate if motifs that regulate presynaptic Ca_V2 subtype abundance are also utilized to determine Ca_V2 subtype preference or if they were

distinct. The remaining Ca^{2+} currents from calyces expressing the $Ca_V2.1/2.3$ chimeras could be mediated by: 1) a mixture of $Ca_V2.1/2.3$ chimeras and $Ca_V2.3$ channels, 2) solely $Ca_V2.1/2.3$ chimeras, or 3) solely $Ca_V2.3$ channels. Since the presynaptic Ca^{2+} currents in the $Ca_V2.1^{-/-}$ /$Ca_V2.2^{-/-}$ calyx of Held were completely Aga insensitive, and the $Ca_V2.1/2.3$ chimeras still maintain Aga binding sites and are the Aga sensitive, we measured Aga sensitivity of Ca^{2+} currents with the $Ca_V2.1/2.3$ chimeras to distinguish between the different possibilities. In scenario 1, the $Ca_V2.1/2.3$ chimeras are localized to the presynaptic membrane but do not completely away or only partially compete away $Ca_V2.3$ channels and would result in a mix of Aga sensitive and insensitive Ca^{2+} currents. In scenario 2, $Ca_V2.1/2.3$ chimeras are localized to the presynaptic membrane and compete away $Ca_V2.3$ channels and would result in similar Aga sensitivity as the $Ca_V2.1$ FT. In scenario 3, $Ca_V2.1/2.3$ chimeras are not localized to the presynaptic membrane with only $Ca_V2.3$ currents remaining and would result in similar Aga insensitivity as the $Ca_V2.1^{-/-}$/ $Ca_V2.2^{-/-}$ calyx of Held. Analysis of Aga sensitivity of $Ca_V2.1/2.3$ II-III or $Ca_V2.1/2.3$ CT showed no difference compared to the $Ca_V2.1$ FT (Fig. 5). However, we found partial Aga sensitivity with $Ca_V2.1/2.3$ II-III+ CT (Aga sensitive fraction (%): $Ca_V2.1$ FT 90.43 ± 5.97 (n=7) vs. $Ca_V2.1/2.3$ II-III+ CT 69.67 ± 12.93 (n=9), p=0.0017) (Fig. 5). Based on our data, we demonstrate that both $Ca_V2.1/2.3$ chimeras with the loop II-III or CT swap are able to compete away $Ca_V2.3$ channels (Fig. 5). Therefore, we conclude that $Ca_V2.1$ loop II-III and the CT do not independently control $Ca_V2.1$ preference and motifs that regulate presynaptic $Ca_V2.1$ preference are distinct from those that regulate presynaptic $Ca_V2.1$ abundance.

The $Ca_V2.3$ α_1 subunit CT negatively regulates presynaptic $Ca_V2.1$ abundance while the $Ca_V2.1$ CT aa. 1933-1966 positively regulates presynaptic $Ca_V2.1$ abundance

The $Ca_V2.3$ CT contains a Calmodulin binding domain (CBD) but does not contain many motifs postulated to mediate presynaptic $Ca_V2.1$ subtype abundance (Kamp *et al.*, 2012; Nanou & Catterall, 2018). In addition, proposed $Ca_V2.1$ CT motifs (aa 2016 onwards) are not essential determinants of presynaptic $Ca_V2.1$ abundance (Lubbert *et al.*, 2017). Thus, we hypothesized

that the 1) $Ca_V2.3$ CT acts as a negative regulator of presynaptic Ca_V2 abundance, and/or 2) the $Ca_V2.1$ CBD regulates presynaptic Ca_V2 abundance. Therefore, to elucidate the mechanism of action of the $Ca_V2.3$ CT, we created two additional $Ca_V2.1/2.3$ CT chimeras. They were the $Ca_V2.1/2.3$ CT 1967-2368, which replaces the $Ca_V2.1$ CT with the $Ca_V2.3$ CT from $Ca_V2.1$ aa. 1967 onwards and contains the $Ca_V2.3$ CBD, and the $Ca_V2.1/2.3$ CT 2016-2368 which replaces the $Ca_V2.1$ CT with the $Ca_V2.3$ CT from $Ca_V2.1$ aa 2016 onwards (Fig. 6A). Subsequently, we expressed these chimeras and $Ca_V2.1$ Δ2016, which deletes all motifs, AZ protein binding sites, and the secondary $Ca_V\beta$ interaction site(Lubbert *et al.*, 2017) and measured their maximum Ca^{2+} amplitudes to determine rescue efficiency (Fig. 6). As previously published. we found no difference in maximum Ca^{2+} currents between $Ca_V2.1$ Δ2016 and $Ca_V2.1$ FT (Fig. 6B-C), thereby confirming that motifs in the $Ca_V2.1$ CT aa. 2016 onwards are not essential for controlling presynaptic $Ca_V2.1$ abundance. In contrast, expression of $Ca_V2.1/2.3$ CT 2016-2368 and $Ca_V2.1/2.3$ CT 1967-2368 resulted in a reduction in the maximum Ca^{2+} current amplitudes ($Ca_V2.1$ Δ2016: -1241 ± 207.4 (n=6) vs. $Ca_V2.1/2.3$ CT 2016-2368: -934.1 ± 210.6 (pA) (n=12), p=0.0209; $Ca_V2.1$ Δ2016: -1241 ± 207.4 (n=6) vs. $Ca_V2.1/2.3$ CT 1967-2368: -839.5 ± 251.9 (pA) (n=8), p=0.0047) (Fig. 6D-F), but the maximum Ca^{2+} current amplitudes with either $Ca_V2.1/2.3$ CT 1967-2368 or $Ca_V2.1/2.3$ CT 2016-2368 were larger than the $Ca_V2.1/2.3$ CT 1933-2368 ((pA) $Ca_V2.1/2.3$ CT aa. 1933-2368: -557.7 ± 198.9 (n=9) vs. $Ca_V2.1/2.3$ CT 2016-2368: -934.1 ± 210.6 (n=12), p=0.0013; $Ca_V2.1/2.3$ CT aa. 1933-2368: -557.7 ± 198.9 (n=9) vs. $Ca_V2.1/2.3$ CT 1967-2368: -839.5 ± 251.9 (n=8), p=0.0321) (Fig. 6D-F). Therefore, we conclude that the $Ca_V2.3$ CT aa. 1952-2273 contains a motif or motifs that negatively regulate presynaptic $Ca_V2.3$ abundance and the $Ca_V2.1$ CBD is not a positive regulator of presynaptic $Ca_V2.1$ abundance. Furthermore, we identified the region between $Ca_V2.1$ CT aa. 1933-1966 positively regulates presynaptic $Ca_V2.1$ abundance.

The $Ca_V2.2$ CT does not control presynaptic $Ca_V2.1$ abundance

Since we identified that the $Ca_V2.3$ CT was a negative regulator of presynaptic $Ca_V2.3$

abundance, we set out to determine if this was unique to the $Ca_V2.3$ CT. Thus, to address if $Ca_V2.2$ CT negatively regulated presynaptic Ca_V2 abundance, we created a $Ca_V2.1/2.2$ CT chimera and cloned this into our HdAd vectors. Western blot analysis demonstrated no issues with expression of the $Ca_V2.1/2.2$ CT chimera (Fig. 7A). Subsequently we expressed the $Ca_V2.1/2.2$ CT chimera and performed IV analysis on presynaptic Ca^{2+} currents. Results of our IV analysis revealed that there was no difference in the maximum Ca^{2+} current between the $Ca_V2.1/2.2$ CT chimera and $Ca_V2.1$ FT (Fig. 7B-E). However, compared to $Ca_V2.1$ FT, there appeared to be unequal variances of maximum Ca^{2+} current amplitudes with $Ca_V2.1/2.2$ CT that was marginally significant (F-test comparing variances p=0.0607) (Fig. 7B-E). Therefore, our data suggests that the $Ca_V2.2$ CT is not a negative regulator of presynaptic abundance.

High level overexpression of $Ca_V2.1/2.2$ CT rescues presynaptic Ca^{2+} currents while $Ca_V2.1/2.3$ CT does not.

High level overexpression of $Ca_V2.1$ α_1 subunit results in increased presynaptic $Ca_V2.1$ levels and compete away $Ca_V2.2$ and $Ca_V2.3$ channels, however high-level overexpression of $Ca_V2.2$ α_1 subunit does not result in a reduction of $Ca_V2.1$ levels at the calyx of Held (Lubbert *et al.*, 2019a). This suggests that upstream regulatory steps, such as protein trafficking and membrane insertion steps, are integral to $Ca_V2.1$ level preference and abundance (Ferron *et al.*, 2021; Young & Veeraraghavan, 2021). It is known that high levels of overexpression can saturate regulatory steps that control trafficking (Lubbert *et al.*, 2019a). Therefore, to determine if these regulatory step(s) could be saturated, we used the high-level overexpression Pun cassette (Young & Neher, 2009; Montesinos *et al.*, 2011; Lubbert *et al.*, 2019a) to drive expression of $Ca_V2.1/2.2$ CT and $Ca_V2.1/2.3$ CT chimeras and determine if we could increase the presynaptic Ca_V2 chimera current levels and compared their maximum Ca^{2+} current amplitudes to Pun $Ca_V2.1$ FT. We found no difference in presynaptic Ca^{2+} currents with Pun $Ca_V2.1/2.2$ CT compared to Pun $Ca_V2.1$ FT (Fig. 8). However, maximum Ca^{2+} current amplitudes with Pun $Ca_V2.1/2.3$ CT were lower than Pun $Ca_V2.1$ FT (Pun $Ca_V2.1$ FT: -1438 ±

198.9 (n=7) vs. Pun $Ca_V2.1/2.3$ CT: -772.8 ± 291.8 (n=10), (pA), p=0.0006) (Fig. 8). Moreover, the maximum Ca^{2+} current amplitudes with Pun $Ca_V2.1/2.3$ CT showed no significant difference than syn $Ca_V2.1/2.3$ CT (Fig. 8). Therefore, we demonstrate that the $Ca_V2.2$ CT is not a negative regulator of presynaptic $Ca_V2.2$ abundance and the $Ca_V2.1/2.2$ CT chimera can be forced to increase expression level, however, the negative regulator motif in $Ca_V2.3$ CT restrains the upstream regulatory steps which results in low abundance of $Ca_V2.3$ channels in the presynaptic terminal.

Discussion

In this study, we provide insight into how presynaptic Ca_V2 subtype abundance is determined by the Ca_V2 α_1 subunit. Based on our data, we demonstrate that the cytoplasmic loop II-III and CT regions of the $Ca_V2.1$ α_1 subunit are positive regulators of presynaptic Ca_V2 abundance, while $Ca_V2.3$ CT negatively regulates presynaptic Ca_V2 abundance. In addition, we find that $Ca_V2.2$ CT is not a key determinant of presynaptic Ca_V2 abundance. Furthermore, we demonstrate that $Ca_V2.1$ α_1 subunit cytoplasmic loop II-III and CT regions do not independently control presynaptic $Ca_V2.1$ preference. Therefore, we propose that the motifs controlling presynaptic $Ca_V2.1$ preference are distinct from those regulating $Ca_V2.1$ levels and they may act synergistically in pathways that regulate presynaptic $Ca_V2.1$ preference and levels.

The Ca_V2 α_1 subunit II-III loop regulation of presynaptic $Ca_V2.1$ abundance.

By swapping the loop II-III domain between $Ca_V2.1$ and $Ca_V2.3$ we demonstrated that the $Ca_V2.1$ loop II-III region positively regulates presynaptic $Ca_V2.1$ abundance but does not regulate preference. All Ca_V2 subunit loop II-III domains contain a synprint region which is the site of interaction between the SNARE proteins syntaxin and SNAP-25 (Zhong *et al.*, 1999; Mochida *et al.*, 2003; Yokoyama *et al.*, 2005). However, the proposed syntaxin binding domain found in $Ca_V2.1$ and $Ca_V2.2$ is not found in the $Ca_V2.3$ α_1 subunit synprint region (Kamp *et al.*, 2005; Yokoyama *et al.*, 2005; Rajapaksha *et al.*, 2008). Therefore, our findings that the $Ca_V2.1/2.3$ loop II-III chimera resulted in presynaptic Ca^{2+} current reductions indicates that potential differences in syntaxin binding between the different subtypes of Ca_V2 α_1 subunits may regulate presynaptic Ca_V2 abundance. Studies from cultured hippocampal neurons, $Ca_V2.1$ dominant presynaptic terminals, found that partial deletions in the $Ca_V2.2$ synprint region that impact SNARE binding resulted in less efficient $Ca_V2.2$ targeting to presynaptic terminal (Szabo *et al.*, 2006). Similar partial deletions in the $Ca_V2.1$ synprint region reduced $Ca_V2.1$ localization to release sites in cultured superior cervical ganglion (SCG) neurons which utilize $Ca_V2.2$ dominant presynaptic terminals (Mochida *et al.*, 2003). In addition, splice variants of $Ca_V2.1$

lacking the synprint region reduce incorporation into neuroendocrine cells (Rajapaksha *et al.*, 2008). Since partial deletions of $Ca_V2.2$ synprint do not impair axonal targeting(Szabo *et al.*, 2006), it is possible that the $Ca_V2.3$ synprint region does not regulate axonal trafficking but rather regulates incorporation into the presynaptic terminal. Although the $Ca_V2.3$ synprint region chimera resulted in reduced presynaptic Ca_V2 chimera levels, there was no change in the proportion of Agatoxin sensitive currents. Therefore, this indicates the mechanisms that control $Ca_V2.1$ preference are not determined by the loop II-III region binding interactions.

An alternative interpretation of our data is that the loop II-III swaps resulted in changes in increased inactivation of the $Ca_V2.1/2.3$ channels which resulted in a reduction in presynaptic Ca^{2+} currents that was unrelated to abundance. However, deletion of the entire synprint site which contains syntaxin and SNAP25 binding sites from the $Ca_V2.1$ α_1 subunit has similar activation and a positive shift in the inactivation curves and there was no difference in normalized conductance at -80 mV and -70 mV (Mochida *et al.*, 2003). Furthermore, $Ca_V2.3$ channels have a half inactivation voltage(Pereverzev *et al.*, 2002) that is similar to $Ca_V2.1$ (Mochida *et al.*, 2003). More importantly, we demonstrated the relative *Po* and N between the $Ca_V2.1/2.3$ loop II-III channels and $Ca_V2.1$ channels were similar in HEK293T cells.

The Ca_V2 α_1 subunit CT differentially regulates presynaptic Ca_V2 subtype abundance.

We found that the $Ca_V2.2$ CT and $Ca_V2.3$ CT had differential effects on presynaptic Ca_V2 abundance but did not impact Ca_V2 preference. Our data demonstrated that $Ca_V2.1/2.3$ CT chimera results in a severe reduction in presynaptic Ca^{2+} currents with no difference in the Po or N. Therefore, our data suggests that the $Ca_V2.3$ CT is a negative regulator of presynaptic $Ca_V2.3$ abundance. Prior studies (Lubbert *et al.*, 2017) and our findings here revealed that the $Ca_V2.1$ CT Δ2016, which deletes multiple AZ protein binding sites and other motifs restores presynaptic Ca^{2+} current levels to $Ca_V2.1$ FT levels. These data demonstrate these interactions and motifs are not essential for controlling presynaptic $Ca_V2.1$ abundance. However, replacing the $Ca_V2.1$ CT from aa. 2016 onwards with corresponding $Ca_V2.3$ CT aa. 1952-2273 resulted in

a reduction of presynaptic Ca^{2+} currents compared to $Ca_V2.1$ CT Δ2016. Furthermore, overexpression of $Ca_V2.1/2.3$ CT chimera by pUNISHER cassette was similar to presynaptic Ca^{2+} currents levels with the low-level synapsin expression cassette. Although it is possible that the $Ca_V2.3$ CT contains motif that alters tonic modulation of the channels, $Ca_V2.3$ channels have a half inactivation voltage (Pereverzev *et al.*, 2002) that is similar to $Ca_V2.1$ (Mochida *et al.*, 2003). Finally, $Ca_V2.3$ levels are significantly less than $Ca_V2.1$ and correspond to limited contribution of $Ca_V2.3$ channels to the presynaptic Ca_V2 current subtype contribution (Wu *et al.*, 1999).

Therefore, we propose that $Ca_V2.3$ CT aa. 1952-2273 contains a motif that prevents presynaptic Ca_V2 targeting or incorporation into the plasma membrane. In addition, our results indicate that CT dependent mechanism of regulation of presynaptic Ca_V2 abundance is dominant to the loop II-III region mechanisms of action as $Ca_V2.1/2.3$ CT chimera resulted in significantly lower presynaptic Ca^{2+} currents than those with the $Ca_V2.1/2.3$ loop II-III.

Calmodulin (CaM) is considered a core component of Ca_V2 channel complexes and interacts with the Cav2.1 channels through a bipartite interaction with the calmodulin binding domain (CBD) and IQ-like motif (IM) domain to regulate calcium dependent facilitation (CDF) and inactivation (CDI) (Lee *et al.*, 2003; Chaudhuri *et al.*, 2004; Mori *et al.*, 2008). However, how CaM interactions regulate presynaptic $Ca_V2.1$ levels is unclear. The $Ca_V2.1/2.3$ CT aa. 1967-2368 chimera, which replaces the $Ca_V2.1$ CBD with the $Ca_V2.3$ CBD, showed no difference in rescuing efficiency compared to $Ca_V2.1/2.3$ CT aa. 2016-2368 chimeras. However, we found that presynaptic Ca^{2+} currents with $Ca_V2.1/2.3$ CT aa. 1967-2368 chimera were larger than that with $Ca_V2.1/2.3$ CT aa. 1933-2368 chimera. Therefore, our results demonstrated that the $Ca_V2.1$ CBD does not control presynaptic $Ca_V2.1$ abundance but the linker region of $Ca_V2.1$ CT aa. 1933-1966 between the IQ domain and the CBD plays a role in regulation of $Ca_V2.1$ levels. Since the CaM/CBD complex interacts with the IM domain (Nanou *et al.*, 2016; Serra *et al.*, 2018), it is possible that the $Ca_V2.3$ CBD and linker region with $Ca_V2.1$ IQ domain result in a

different structural conformation of the CT that impacts presynaptic Ca_V2 abundance. Interestingly, the combination of the mutation (IM-AA) in the IM domain and CBD deletion in SCG neurons results in an increased peak Ca^{2+} currents levels, while the IM-AA or CBD deletion alone did not alter Ca^{2+} current levels (Mochida *et al.*, 2008). Therefore, the IQ domain and CBD may synergistically regulate $Ca_V2.1$ level. However, the molecular mechanisms how these regions impact $Ca_V2.1$ abundance is unknown and future experiments are needed.

In contrast to the $Ca_V2.1/2.3$ CT chimera, we found no difference in the average presynaptic Ca^{2+} current levels with the $Ca_V2.1/2.2$ CT chimera compared to $Ca_V2.1$ FT. However, we observed a large variability of Ca^{2+} current amplitudes with $Ca_V2.1/2.2$ CT that is marginally significant compared to $Ca_V2.1$ FT rescue. Therefore, our data implies that the $Ca_V2.2$ CT is not a key determinant of presynaptic Ca_V2 abundance. Unlike the $Ca_V2.3$ CT, high level overexpression of $Ca_V2.1/2.2$ CT resulted in similar presynaptic Ca^{2+} current levels compared to high level overexpression of $Ca_V2.1$ FT level and no change in variability. Therefore, we propose that the $Ca_V2.2$ CT does not contain motifs that prevents presynaptic $Ca_V2.2$ targeting or incorporation into the plasma membrane.

Ca_V2 subtype abundance and preference are regulated by distinct pathways.

Although there were differences in the presynaptic Ca^{2+} current levels with the $Ca_V2.1/2.3$ loop II-III and $Ca_V2.1/2.3$ CT chimeras, they had similar Aga sensitivity as presynaptic Ca^{2+} currents with the $Ca_V2.1$ FT. However, there was a significant Aga insensitive component of Ca^{2+} currents with $Ca_V2.1/2.3$ loop II-III+ CT chimera despite having similar Ca^{2+} current levels as the $Ca_V2.1/2.3$ CT and $Ca_V2.1^{-/-}$/ $Ca_V2.2^{-/-}$ background. Therefore, our data indicates that: 1) Presynaptic Ca_V2 subtype abundance mechanisms are independent of those that control preference. 2) The loop II-III region and the CT region do not individually encode preference. 3) The $Ca_V2.1$ II-III loop and CT region may act synergistically to control Ca_V2 subtype preference. 4) Other motifs in the $Ca_V2.1$ α_1 subunit outside of the CT and synprint region are involved in regulating presynaptic Ca_V2 subtype preference. Potential candidates that

may control preference are the Ca_V2 α_1 subunit at AID in domain I-II which binds to the $Ca_V\beta$ subunit with high affinity(De Waard *et al.*, 1994). $Ca_V\beta$ subunits are critical for regulating Ca_V2 trafficking and $Ca_V\beta4$ and $Ca_V\beta2a$ are located within the presynaptic terminal. $Ca_V2.1$ channels have higher specificity for binding to $Ca_V\beta4$ than $Ca_V2.2$ and $Ca_V2.3$ channels (Xie *et al.*, 2007; Muller *et al.*, 2010). Another possibility is that preference is not encoded by motifs in the cytoplasmic regions but is controlled by the Cacna2d protein family (Dolphin, 2012; Hoppa *et al.*, 2012; Stephani *et al.*, 2019). Knockout of $\alpha_2\delta3$ subunit in spiral ganglion neurons results in reduced $Ca_V2.1$ and $Ca_V2.3$ components with no change in $Ca_V2.2$ subtype levels (Stephani *et al.*, 2019). In contrast overexpression of $\alpha_2\delta1$ subunit decreases $Ca_V2.2$ level in cultured hippocampal neurons (Pilch *et al.*, 2022), but did not change other Ca_V2 subtype levels. Furthermore, the globular bushy cells which give rise to the calyx of Held, only express *Cacna2d2* and *Cacna2d3*. In addition, other synapses that undergo developmental reduction of $Ca_V2.2$ and $Ca_V2.3$ express *Cacna2d1*. Finally, the $\alpha_2\delta$ binding preference does not correlate to presynaptic Ca_V2 subtype levels (Voigt *et al.*, 2016) while CACNA2D expression patterns do not correlate to presynaptic Cav2 subytpe levels (Cole *et al.*, 2005). Therefore, given these conflicting findings more experiments will be needed to decipher if the Cacna2d proteins regulate preference.

While it is possible that the loop II-III domain and the CT domain act in concert to regulate presynaptic preference, it is also possible that they are not involved in preference mechanisms but rather combination of the loop II-III and CT domain swap construct dramatically impair the Ca_V2 chimera trafficking to the presynaptic terminal. In this scenario, the $Ca_V2.1/2.3$ II-III loop+ CT chimera does not effectively compete away native $Ca_V2.3$ channels, which are normally restricted from the upstream pathways that regulate presynaptic trafficking. Therefore, native $Ca_V2.3$ channels are also trafficked to the presynaptic terminals that express the $Ca_V2.1/2.3$ II-III loop+ CT chimera. In this hypothetical scenario, the preference mechanism(s) has high affinity for the $Ca_V2.1/2.3$ chimera channel and low affinity for the $Ca_V2.3$ channels,

however by law of mass action, $Ca_V2.3$ channels now participate in molecular pathways that determine preference and results in the presence of presynaptic $Ca_V2.3$ channels. Based on our model, this demonstrates how alternative splicing of the Ca_V2 α_1 subunits and potentially alternative splicing of molecules in pathways that control Ca_V2 trafficking (Weiss & Zamponi, 2017), and insertion into the membrane may lead to developmentally changes in presynaptic Ca_V2 subtype levels. However, the molecular machinery and the motifs that determine preference remain to be identified.

Limitations of our study

By generating our $Ca_V2.1$ chimeric constructs and expressing them at the calyx of Held we identified regions in the Ca_V2 α_1 subunit that control presynaptic Ca_V2 abundances based on changes in presynaptic Ca^{2+} currents levels. However, although we did not directly measure N presynaptic Ca^{2+} currents directly correlates to changes in presynaptic Ca^{2+} channel abundance (Holderith *et al.*, 2012; Nakamura *et al.*, 2015; Nusser, 2018; Lubbert *et al.*, 2019a; Rebola *et al.*, 2019; Radulovic *et al.*, 2020). Therefore, an alternate hypothesis is that measures of whole cell presynaptic Ca^{2+} currents do not reflect changes in presynaptic Ca^{2+} channel abundance but rather changes in intrinsic biophysical properties of the chimeric channels that result in reduced presynaptic Ca_V2 channel activity, or differences in related to general mechanisms trafficking or translation. However, measurements in HEK293T cells showed no change in the peak currents between the $Ca_V2.1/2.3$ chimeras and no change in the relative *Po* and N of the chimeric constructs in HEK293T cells. Moreover, all Ca_V2 chimeras cDNA sequences were codon optimized and identical transgene cassettes were used to express these constructs. Therefore, reduced presynaptic Ca^{2+} currents are not due to changes of intrinsic biophysical properties, Po or translation levels. More importantly, this supports that the reductions in presynaptic Ca^{2+} currents reflect changes in presynaptic Ca_V2 channel abundance. Finally, studies did not determine the exact molecular mechanism, such as channel trafficking, insertion, retention, that control presynaptic abundance but have identified specific motifs in the Ca_V2 α_1

subunit. Future studies will be needed to determine these steps. However, while presynaptic terminals appear to have a ceiling for total amount of calcium channels (Cao *et al.*, 2004; Holderith *et al.*, 2012; Nakamura *et al.*, 2015; Nusser, 2018; Lubbert *et al.*, 2019b; Rebola *et al.*, 2019), specific slots for distinct channel subtypes in the presynaptic terminal do not exist (Lubbert *et al.*, 2019b).

All in all, by demonstrating that motifs in the Ca_V2 α_1 subunit that control presynaptic Ca_V2 subtype abundance are distinct from those determining presynaptic Ca_V2 subtype preference, our findings provide new insights into the regulation of presynaptic Ca_V2 subtype levels.

Figure legends

Figure 1. Presynaptic $Ca_V2.1$ and $Ca_V2.2$ channels can be ablated and the remaining Ca^{2+} currents are compensated by $Ca_V2.3$ channels at the calyx of Held.

(A) Illustration of CKO mouse model. Exon 4 of *Cacna1a*, and exons 5 and 6 of *Cacna1b* are flanked by LoxP sites. (B-C) Example traces of Ca^{2+} currents and bar graph show rundown fraction of electrophysiological recordings at duration of 10~15min at wildtype calyx of Held (n=3). (D) Pharmacological isolation of presynaptic Ca_V2 isoforms in wildtype and $Ca_V2.1^{-/-}$/ $Ca_V2.2^{-/-}$ calyces. Ca^{2+} current traces in absence of any blockers (black), after blocking $Ca_V2.1$ fraction with 200 nM Aga (orange), after blocking $Ca_V2.2$ fraction with 2 mM Cono (blue) and after blocking all Ca_V channels with 50 mM Cd^{2+} (gray). (E) Bar graph shows total Ca^{2+} currents in wildtype and $Ca_V2.1^{-/-}$/ $Ca_V2.2^{-/-}$ calyces. (F) Relative Ca_V2 subtype fractions in wildtype, $Ca_V2.1^{-/-}$/ $Ca_V2.2^{-/-}$ calyces (n=3-5 for each condition). (G) Ca^{2+} current traces in absence of any blockers (black), after blocking $Ca_V2.3$ fraction with 200 nM SNX-482 (green). (H) Bar graph shows SNX-482 sensitive fraction at $Ca_V2.1^{-/-}$/ $Ca_V2.2^{-/-}$ calyces (n=3). (I) Ca^{2+} current traces in absence of any blockers (black), after blocking Ca_V1 fraction with 10 μM Nifedipine (red). (J) Bar graph shows the reduction fraction and Ca^{2+} current amplitudes in $Ca_V2.1^{-/-}$/ $Ca_V2.2^{-/-}$ calyces after Nifedipine treatment compared to wildtype rundown fraction.

Figure 2. $Ca_V2.1/Ca_V2.3$ Chimeras can be efficiently expressed.

Western Blot validated protein expression of Ca_V2 hybrid constructs. HEK293 cells are infected by HdAd $Ca_V2.1/2.3$ chimeric constructs. (A) Illustration of Ca_V2 α_1 structure. Four transmembrane domains are highly conserved while the cytoplasmic loops are highly variant between $Ca_V2.1$ and $Ca_V2.3$, the I-II loop, II-III loop and CT share 87.3%, 33.2% and 39.8% consensus, respectively. (B) Illustration of swapped region between $Ca_V2.1$ and $Ca_V2.3$ channels, the amino acid numbers are labelled. (C) Illustration of three $Ca_V2.1/2.3$ chimeric constructs. $Ca_V2.1$ II-III loop and CT are both replaced by $Ca_V2.3$ II-III loop and CT in $Ca_V2.1/2.3$ II-III loop + CT chimeric construct. $Ca_V2.1$ II-III loop is replaced by $Ca_V2.3$ II-III loop in

$Ca_V2.1/2.3$ II-III loop chimeric construct. $Ca_V2.1$ CT is replaced by $Ca_V2.3$ CT in $Ca_V2.1/2.3$ CT chimeric construct. (D) Antibody targeting $Ca_V2.1$ CT shows the protein expression of $Ca_V2.1$ FT and $Ca_V2.1/2.3$ II-III loop. (E) Antibody targeting $Ca_V2.1$ II-III loop fails to detect protein expression of $Ca_V2.1/2.3$ II-III loop and $Ca_V2.1/2.3$ II-III loop CT, indicating that the II-III loop of $Ca_V2.1$ is swapped by $Ca_V2.3$ II-III loop. (F) Antibody targeting $Ca_V2.3$ CT shows the protein expression of $Ca_V2.1/2.3$ II-III loop CT and $Ca_V2.1/2.3$ CT. Mock, negative control, protein lysis from uninfected HEK293 cells.

Figure 3. The $Ca_V2.1/2.3$ α_1 CT chimera cannot rescue Ca^{2+} currents to $Ca_V2.1$ FT levels, however the $Ca_V2.1/2.3$ loop II-III chimera partially rescues Ca^{2+} currents.

Sample traces of Ca^{2+} current triggered by 50 ms voltage steps from -60 mV to -30 mV in 10 mV steps, -25 mV to +20 mV in 5 mV steps, and +30 mV to +60 mV in 10 mV steps. Black: calyces expressing $Ca_V2.1$ FT (n=11). Yellow: $Ca_V2.1^{-/-}$/ $Ca_V2.2^{-/-}$ calyces (n=11). Red: calyces expressing $Ca_V2.1/2.3$ II-III loop CT chimeric construct (n=8). Blue: calyces expressing $Ca_V2.1/2.3$ II-III loop chimeric construct (n=11). Gray: calyces expressing $Ca_V2.1/2.3$ CT chimeric construct (n=9). (B-C) IV relationship of Ca^{2+} currents (B) and normalized Ca^{2+} currents by maximal Ca^{2+} currents (I/I_{max}; C) plotted against voltage steps. (D-E) Bar graph shows absolute peak Ca^{2+} current amplitudes, one-way ANOVA, Dunnett's test, $Ca_V2.1$ FT is used as positive control (D) and $Ca_V2.1^{-/-}$/ $Ca_V2.2^{-/-}$ is used as negative control (E). (F-G) Bar graph shows voltage dependent activation kinetics of Ca_V2 chimeras. Half-maximal activation voltage (V_m) (F) and voltage-dependence of activation (K_m) (G) is plotted. One-way ANOVA, Dunnett's test, $Ca_V2.1$ FT is used as positive control.

Figure 4. Ca_V2 chimeras have similar expression level and open probability in HEK293T cells.

(A) CMV promoter is used to drive Ca_V2 chimera expressions in HEK293T cells. Example Ca^{2+} current traces to 10ms depolarization from -80mV holding potential to the reverse potential

+50mV for HEK293T cells transfected with CMV $Ca_V2.1$ FT (black, n=11), CMV $Ca_V2.1/2.3$ II-III loop CT (dark red, n=13), CMV $Ca_V2.1/2.3$ II-III loop (blue, n=12), CMV $Ca_V2.1/2.3$ CT (gray, n=10) and CMV $Ca_V2.1$ FT without CMV $Ca_V\beta4$ co-expression (red, n=7). (B-C) Bar graph shows Q_{max} (B) and linear regression plots (C) shows ratio between I_{tail} and Q_{max} in HEK293T cells co-transfected with CMV Ca_V2 chimeras and CMV $Ca_V\beta4$.

Figure 5. The $Ca_V2.1/2.3$ $\alpha_1$subunit chimeras compete away $Ca_V2.3$ channel in the calyx of Held.

(A) Agatoxin isolation of presynaptic $Ca_V2.1/2.3$ chimeras in calyces expressing $Ca_V2.1$ FT (black, n=7), $Ca_V2.1/2.3$ II-III loop CT (red, n=9), $Ca_V2.1/2.3$ II-III loop (blue, n=7), and $Ca_V2.1/2.3$ CT (gray, n=8). Basal and reduced Ca^{2+} current traces after applying 200 nM ω-Aga IVA are labelled. (B) Reduction of Agatoxin sensitive Ca^{2+} current over time. Ca^{2+} current amplitudes are plotted against time, 200 nM ω-Aga IVA was applied at 5th pulse (50s). (C) Bar graph shows the ω-Aga IVA sensitive reduction fraction in calyces expressing $Ca_V2.1$ FT, $Ca_V2.1/2.3$ II-III loop CT, $Ca_V2.1/2.3$ II-III loop, and $Ca_V2.1/2.3$ CT.

Figure 6. The $Ca_V2.3$ CT negatively regulates presynaptic Ca_V2 abundance, while the $Ca_V2.1$ CT region aa. 1933-1966 promotes $Ca_V2.1$ abundance.

(A) Amino acid alignment of $Ca_V2.1$ and $Ca_V2.3$ CT. Sequences on top and bottom represent $Ca_V2.1$ CT and $Ca_V2.3$ CT, respectively. Amino acid numbers of swapped sites in three $Ca_V2.1/2.3$ chimeras are indicated in black. $Ca_V2.1$ CBD is highlighted in green. (B) Example Ca^{2+} current traces to 50 ms depolarization from -80mV holding potential to the maximal activation voltage step (-15mV to +15mV, 5 mV steps) for $Ca_V2.1$ FT (black, n=11) and $Ca_V2.1$ Δ2016 (red, n=6). (C) Bar graph shows absolute peak Ca^{2+} currents amplitude between $Ca_V2.1$ CT and $Ca_V2.1$ Δ2016, unpaired t test. (D) Example Ca^{2+} current traces to 50ms depolarization from -80mV holding potential to the maximal activation voltage step (-15mV to +15mV, 5 mV steps) for $Ca_V2.1$ Δ2016, $Ca_V2.1/2.3$ CT aa. 2016-2368 (n=12); $Ca_V2.1/2.3$ CT 1967-2368 (n=8)

and $Ca_V2.1/2.3$ CT 1933-2368 (n=9). (E-F) Bar graph shows peak Ca^{2+} currents amplitude, one-way ANOVA, Dunnett's test, $Ca_V2.1$ Δ2016 is used as positive control (E) and $Ca_V2.1/2.3$ CT aa. 1933-2368 is used as negative control (F).

Figure 7. $Ca_V2.1/2.2$ CT chimera can be efficiently expressed and rescues Ca^{2+} currents to $Ca_V2.1$ FT level with high variability.

(A) Western Blot validated protein expression of $Ca_V2.1/2.2$ CT. HEK293 cells are infected by HdAd $Ca_V2.1/2.2$ CT and $Ca_V2.2$ FT. Antibody targeting $Ca_V2.2$ CT shows the protein expression of $Ca_V2.2$ FT and $Ca_V2.1/2.2$ CT. Mock, negative control, protein lysis from uninfected HEK293 cells. (B) Exemplary Ca^{2+} currents triggered by 50 ms voltage steps from -60 mV to -30 mV in 10 mV steps, -25 mV to +20 mV in 5 mV steps, and +30 mV to +60 mV in 10 mV steps. Black: calyces expressing $Ca_V2.1$ FT (n=11). Yellow: $Ca_V2.1^{-/-}$/ $Ca_V2.2^{-/-}$ calyces (n=11). Green: calyces expressing $Ca_V2.1/2.2$ CT (n=11). (C-D) IV relationship of Ca^{2+} currents (C) and normalized Ca^{2+} currents by maximal Ca^{2+} currents (I/I_{max}; D) plotted against voltage steps. (E) Bar graph shows absolute peak Ca^{2+} current amplitudes. One-way ANOVA, Dunnett's test, $Ca_V2.1$ FT is used as positive control, $Ca_V2.1^{-/-}$/ $Ca_V2.2^{-/-}$ is used as negative control.

Figure 8. High level overexpression of the $Ca_V2.1/2.3$ α_1 CT cannot rescue Ca^{2+} currents to Pun $Ca_V2.1$ levels while Pun $Ca_V2.1/2.2$ α_1 CT can.

(A) High-level overexpression cassette pUNISHER (Pun) is used to drive $Ca_V2.1$ FT, $Ca_V2.1/2.2$ CT and $Ca_V2.1/2.3$ CT chimeric constructs. Example Ca^{2+} current traces to 50ms depolarization from -80mV holding potential to the maximal activation voltage step (-15mV to +15mV, 5 mV steps) for calyces expressing Pun $Ca_V2.1$ FT (green, n=7), Pun $Ca_V2.1/2.2$ CT (purple, n=9) and Pun $Ca_V2.1/2.3$ CT (orange, n=10). (B) Bar graph shows averaged peak Ca^{2+} currents for Pun $Ca_V2.1$ FT, Pun $Ca_V2.1/2.2$ CT and Pun $Ca_V2.1/2.3$ CT constructs. One-way ANOVA, Dunnett's test, Pun $Ca_V2.1$ FT is used as positive control.

Table1. *Cacna1a, Cacna1b* $^{flox/flox}$ animal characterization.

Parameter	Mean	SD	n	P	statistics
Wildtype animal					
Agatoxin sensitive fraction (%)	79.09	14.98	4		
Agatoxin sensitive currents (pA)	809.3	255.6	4	control	
Conotoxin sensitive fraction (%)	7.828	10.5	4		
Conotoxin sensitive currents (pA)	92.00	142.2	4		
$Ca_V2.1^{-/-}$/ $Ca_V2.2^{-/-}$					
Agatoxin sensitive fraction (%)	13.64	6.24	5	p<0.0001 (****)	
Agatoxin sensitive currents (pA)	99.22	53.64	5	p=0.0005 (***)	
Conotoxin sensitive fraction (%)	11.92	4.722	5	p=0.4571	Unpaired t test
Conotoxin sensitive currents (pA)	50.80	43.10	5	p=0.5532	
SNX-482 sensitive fraction (%)	24.33	9.074	3		
SNX-482 sensitive currents (pA)	86.65	31.26	3		
Rundown fraction					
Wildtype animal (pA)	43.70	20.85	3	control	Unpaired t test
$Ca_V2.1^{-/-}$/ $Ca_V2.2^{-/-}$ (pA)	51.40	23.78	3		
Wildtype animal (%)	3.167	0.6525	3	control	Unpaired t test
$Ca_V2.1^{-/-}$/ $Ca_V2.2^{-/-}$ (%)	8.393	4.169	3	P=0.0985	

Table2. Electrophysiological parameters of IV relations of Ca^{2+} currents.

Parameter	Mean	SD	n	P	statistics
Boltzmann fit: Half-maximal activation voltage $V_{0.5}$ (mV)					
$Ca_V2.1$ FT (control)	-17.29	4.761	11	control	One-Way ANOVA
$Ca_V2.1^{-/-}$/ $Cav2.2^{-/-}$	-14.82	5.428	11	p=0.7135 (n.s.)	Dunnett's test
Cav2.1/2.3 II-III loop CT	-11.25	6.953	8	p=0.0924 (n.s.)	One-Way ANOVA
Cav2.1/2.3 II-III loop	-14.25	5.943	11	p=0.5513 (n.s.)	Dunnett's test
Cav2.1/2.3 CT	-11.34	5.750	9	p=0.0841 (n.s.)	
Boltzmann fit: Voltage-dependence K (mV)					
$Ca_V2.1$ FT (control)	5.052	5.07	11	positive control	
$Ca_V2.1^{-/-}$/ $Cav2.2^{-/-}$	5.756	2.624	11	p=0.9880 (n.s.)	One-Way ANOVA
Cav2.1/2.3 II-III loop CT	6.670	4.116	8	p=0.8508 (n.s.)	Dunnett's test
Cav2.1/2.3 II-III loop	6.628	4.506	11	p=0.8231 (n.s.)	

Cav2.1/2.3 CT	7.556	5.261	9	p=0.5365 (n.s.)

Table3. Capacitances of calyx of Held expressing Ca_V2 hybrid channels.

Parameter	Mean	SD	n	P	statistics
Membrane capacitance C_{slow} (pF)					
Wildtype (control)	20.59	4.220	10	p=0.9246 (n.s.)	
$Ca_V2.1$ FT	23.80	5.150	11	control	
$Ca_V2.1^{-/-}$/ $Cav2.2^{-/-}$	22.85	8.831	11	p=0.9996 (n.s.)	
Cav2.1/2.3 II-III loop CT	21.72	6.096	8	p=0.9990 (n.s.)	
Cav2.1/2.3 II-III loop	25.76	6.045	11	p=0.9960 (n.s.)	One-Way ANOVA
Cav2.1/2.3 CT	19.06	4.894	9	p=0.6135 (n.s.)	Dunnett's Test
$Ca_V2.1$ Δ2016	27.26	3.420	6	p=0.9522 (n.s.)	
Cav2.1/2.3 CT 2016-2368	28.22	7.622	12	p=0.6103 (n.s.)	
Cav2.1/2.3 CT 1967-2368	27.47	8.513	9	p=0.8646 (n.s.)	
Cav2.1/2.2 CT	21.94	9.095	11	p=0.9991 (n.s.)	
Pun $Ca_V2.1$ FT	21.44	5.828	7	p=0.9955 (n.s.)	
Pun $Ca_V2.1$/2.2 CT	23.94	4.943	9	p>0.9999 (n.s.)	
Pun $Ca_V2.1$/2.3 CT	26.04	7.309	10	p=0.9916 (n.s.)	

References

Bewig B & Schmidt WE. (2000). Accelerated titering of adenoviruses. *Biotechniques* **28,** 870-873.

Cao YQ, Piedras-Renteria ES, Smith GB, Chen G, Harata NC & Tsien RW. (2004). Presynaptic Ca2+ channels compete for channel type-preferring slots in altered neurotransmission arising from Ca2+ channelopathy. *Neuron* **43,** 387-400.

Chaudhuri D, Chang SY, DeMaria CD, Alvania RS, Soong TW & Yue DT. (2004). Alternative splicing as a molecular switch for Ca2+/calmodulin-dependent facilitation of P/Q-type Ca2+ channels. *J Neurosci* **24,** 6334-6342.

Chen ZX, Cooper B, Kalla S, Varoqueaux F & Young SM. (2013). The Munc13 Proteins Differentially Regulate Readily Releasable Pool Dynamics and Calcium-Dependent Recovery at a Central Synapse. *Journal of Neuroscience* **33,** 8336-8351.

Cole RL, Lechner SM, Williams ME, Prodanovich P, Bleicher L, Varney MA & Gu G. (2005). Differential distribution of voltage-gated calcium channel alpha-2 delta (alpha2delta) subunit mRNA-containing cells in the rat central nervous system and the dorsal root ganglia. *The Journal of comparative neurology* **491,** 246-269.

De Waard M, Pragnell M & Campbell KP. (1994). Ca2+ channel regulation by a conserved beta subunit domain. *Neuron* **13,** 495-503.

Dolphin AC. (2012). Calcium channel auxiliary alpha2delta and beta subunits: trafficking and one step beyond. *Nat Rev Neurosci* **13,** 542-555.

Dolphin AC & Lee A. (2020). Presynaptic calcium channels: specialized control of synaptic neurotransmitter release. *Nat Rev Neurosci* **21,** 213-229.

Dong W, Radulovic T, Goral RO, Thomas C, Suarez Montesinos M, Guerrero-Given D, Hagiwara A, Putzke T, Hida Y, Abe M, Sakimura K, Kamasawa N, Ohtsuka T & Young SM, Jr. (2018). CAST/ELKS Proteins Control Voltage-Gated Ca(2+) Channel Density and Synaptic Release Probability at a Mammalian Central Synapse. *Cell reports* **24,** 284-293 e286.

Doughty JM, Barnes-Davies M, Rusznak Z, Harasztosi C & Forsythe ID. (1998). Contrasting Ca2+ channel subtypes at cell bodies and synaptic terminals of rat anterioventral cochlear bushy neurones. *J Physiol* **512 (Pt 2),** 365-376.

Eggermann E, Bucurenciu I, Goswami SP & Jonas P. (2011). Nanodomain coupling between Ca(2)(+) channels and sensors of exocytosis at fast mammalian synapses. *Nat Rev Neurosci* **13,** 7-21.

Ferron L, Koshti S & Zamponi GW. (2021). The life cycle of voltage-gated Ca(2+) channels in neurons: an update on the trafficking of neuronal calcium channels. *Neuronal Signal* **5,** NS20200095.

Gandini MA, Sandoval A & Felix R. (2014a). Whole-cell patch-clamp recording of recombinant voltage-sensitive Ca2+ channels heterologously expressed in HEK-293 cells. *Cold Spring Harb Protoc* **2014,** 396-401.

Gandini MA, Sandoval A & Felix R. (2014b). Whole-cell patch-clamp recordings of Ca2+ currents from isolated neonatal mouse dorsal root ganglion (DRG) neurons. *Cold Spring Harbor protocols* **2014,** 389-395.

Giugovaz-Tropper B, Gonzalez-Inchauspe C, Di Guilmi MN, Urbano FJ, Forsythe ID & Uchitel OD. (2011). P/Q-type calcium channel ablation in a mice glycinergic synapse mediated by multiple types of Ca(2)+ channels alters transmitter release and short term plasticity. *Neuroscience* **192,** 219-230.

Holderith N, Lorincz A, Katona G, Rozsa B, Kulik A, Watanabe M & Nusser Z. (2012). Release probability of hippocampal glutamatergic terminals scales with the size of the active zone. *Nat Neurosci* **15,** 988-997.

Hoppa MB, Lana B, Margas W, Dolphin AC & Ryan TA. (2012). alpha2delta expression sets presynaptic calcium channel abundance and release probability. *Nature* **486,** 122-125.

Inchauspe CG, Martini FJ, Forsythe ID & Uchitel OD. (2004). Functional compensation of P/Q by N-type channels blocks short-term plasticity at the calyx of Held presynaptic terminal. *J Neurosci* **24,** 10379-10383.

Iwasaki S, Momiyama A, Uchitel OD & Takahashi T. (2000). Developmental changes in calcium channel types mediating central synaptic transmission. *J Neurosci* **20,** 59-65.

Iwasaki S & Takahashi T. (1998). Developmental changes in calcium channel types mediating synaptic transmission in rat auditory brainstem. *J Physiol* **509 (Pt 2),** 419-423.

Jun K, Piedras-Renteria ES, Smith SM, Wheeler DB, Lee SB, Lee TG, Chin H, Adams ME, Scheller RH, Tsien RW & Shin HS. (1999). Ablation of P/Q-type Ca(2+) channel currents, altered synaptic transmission, and progressive ataxia in mice lacking the alpha(1A)-subunit. *Proc Natl Acad Sci U S A* **96,** 15245-15250.

Kaja S, Van de Ven RC, Ferrari MD, Frants RR, Van den Maagdenberg AM & Plomp JJ. (2006). Compensatory contribution of Cav2.3 channels to acetylcholine release at the neuromuscular junction of tottering mice. *J Neurophysiol* **95,** 2698-2704.

Kamp MA, Krieger A, Henry M, Hescheler J, Weiergraber M & Schneider T. (2005). Presynaptic 'Ca_V2.3-containing' E-type Ca^{2+} channels share dual roles during neurotransmitter release. *Eur J Neurosci* **21,** 1617-1625.

Kamp MA, Shakeri B, Tevoufouet EE, Krieger A, Henry M, Behnke K, Herzig S, Hescheler J, Radhakrishnan K, Parent L & Schneider T. (2012). The C-terminus of human Ca_V2.3 voltage-gated calcium channel interacts with alternatively spliced calmodulin-2 expressed in two human cell lines. *Biochim Biophys Acta* **1824,** 1045-1057.

Lee A, Zhou H, Scheuer T & Catterall WA. (2003). Molecular determinants of Ca(2+)/calmodulin-dependent regulation of Ca(v)2.1 channels. *Proc Natl Acad Sci U S A* **100,** 16059-16064.

Lubbert M, Goral RO, Keine C, Thomas C, Guerrero-Given D, Putzke T, Satterfield R, Kamasawa N & Young SM, Jr. (2019a). Ca(V)2.1 alpha(1) Subunit Expression Regulates Presynaptic Ca(V)2.1 Abundance and Synaptic Strength at a Central Synapse. *Neuron* **101,** 260-273 e266.

Lubbert M, Goral RO, Keine C, Thomas C, Guerrero-Given D, Putzke T, Satterfield R, Kamasawa N & Young SM, Jr. (2019b). CaV2.1 alpha1 Subunit Expression Regulates Presynaptic CaV2.1 Abundance and Synaptic Strength at a Central Synapse. *Neuron* **101,** 260-273 e266.

Lubbert M, Goral RO, Satterfield R, Putzke T, van den Maagdenberg AM, Kamasawa N & Young SM, Jr. (2017). A novel region in the Ca(V)2.1 alpha(1) subunit C-terminus regulates fast synaptic vesicle fusion and vesicle docking at the mammalian presynaptic active zone. *Elife* **6**.

Mochida S, Few AP, Scheuer T & Catterall WA. (2008). Regulation of presynaptic Ca(V)2.1 channels by Ca2+ sensor proteins mediates short-term synaptic plasticity. *Neuron* **57,** 210-216.

Mochida S, Westenbroek RE, Yokoyama CT, Zhong H, Myers SJ, Scheuer T, Itoh K & Catterall WA. (2003). Requirement for the synaptic protein interaction site for reconstitution of synaptic transmission by P/Q-type calcium channels. *Proc Natl Acad Sci U S A* **100,** 2819-2824.

Montesinos MS, Chen ZX & Young SM. (2011). pUNISHER: a high-level expression cassette for use with recombinant viral vectors for rapid and long term in vivo neuronal expression in the CNS. *J Neurophysiol* **106,** 3230-3244.

Montesinos MS, Satterfield R & Young SM, Jr. (2016). Helper-Dependent Adenoviral Vectors and Their Use for Neuroscience Applications. *Methods Mol Biol* **1474,** 73-90.

Mori MX, Vander Kooi CW, Leahy DJ & Yue DT. (2008). Crystal structure of the CaV2 IQ domain in complex with Ca2+/calmodulin: high-resolution mechanistic implications for channel regulation by Ca2+. *Structure* **16,** 607-620.

Muller CS, Haupt A, Bildl W, Schindler J, Knaus HG, Meissner M, Rammner B, Striessnig J, Flockerzi V, Fakler B & Schulte U. (2010). Quantitative proteomics of the Cav2 channel nano-environments in the mammalian brain. *Proc Natl Acad Sci U S A* **107,** 14950-14957.

Nakamura Y, Harada H, Kamasawa N, Matsui K, Rothman JS, Shigemoto R, Silver RA, DiGregorio DA & Takahashi T. (2015). Nanoscale distribution of presynaptic Ca(2+) channels and its impact on vesicular release during development. *Neuron* **85,** 145-158.

Nanou E & Catterall WA. (2018). Calcium Channels, Synaptic Plasticity, and Neuropsychiatric Disease. *Neuron* **98,** 466-481.

Nanou E, Yan J, Whitehead NP, Kim MJ, Froehner SC, Scheuer T & Catterall WA. (2016). Altered short-term synaptic plasticity and reduced muscle strength in mice with impaired

regulation of presynaptic CaV2.1 Ca2+ channels. *Proc Natl Acad Sci U S A* **113,** 1068-1073.

Nusser Z. (2018). Creating diverse synapses from the same molecules. *Curr Opin Neurobiol* **51,** 8-15.

Palmer DJ & Ng P. (2005). Helper-dependent adenoviral vectors for gene therapy. *Human gene therapy* **16,** 1-16.

Pereverzev A, Leroy J, Krieger A, Malecot CO, Hescheler J, Pfitzer G, Klockner U & Schneider T. (2002). Alternate splicing in the cytosolic II-III loop and the carboxy terminus of human E-type voltage-gated Ca(2+) channels: electrophysiological characterization of isoforms. *Mol Cell Neurosci* **21,** 352-365.

Pilch KS, Ramgoolam KH & Dolphin AC. (2022). Involvement of Ca(V) 2.2 channels and alpha(2) delta-1 in homeostatic synaptic plasticity in cultured hippocampal neurons. *J Physiol* **600,** 5333-5351.

Radulovic T, Dong W, Goral RO, Thomas CI, Veeraraghavan P, Montesinos MS, Guerrero-Given D, Goff K, Lubbert M, Kamasawa N, Ohtsuka T & Young SM. (2020). Presynaptic development is controlled by the core active zone proteins CAST/ELKS. *J Physiol-London* **598,** 2431-2452.

Rajapaksha WR, Wang D, Davies JN, Chen L, Zamponi GW & Fisher TE. (2008). Novel splice variants of rat CaV2.1 that lack much of the synaptic protein interaction site are expressed in neuroendocrine cells. *The Journal of biological chemistry* **283,** 15997-16003.

Rebola N, Reva M, Kirizs T, Szoboszlay M, Lorincz A, Moneron G, Nusser Z & DiGregorio DA. (2019). Distinct Nanoscale Calcium Channel and Synaptic Vesicle Topographies Contribute to the Diversity of Synaptic Function. *Neuron* **104,** 693-710 e699.

Rothman JS & Silver RA. (2018). NeuroMatic: An Integrated Open-Source Software Toolkit for Acquisition, Analysis and Simulation of Electrophysiological Data. *Front Neuroinform* **12,** 14.

Serra SA, Gene GG, Elorza-Vidal X & Fernandez-Fernandez JM. (2018). Cross talk between beta subunits, intracellular Ca(2+) signaling, and SNAREs in the modulation of Ca(V) 2.1 channel steady-state inactivation. *Physiol Rep* **6**.

Simms BAZ, G. W. (2014). Neuronal voltage-gated calcium channels: structure, function, and dysfunction. *Neuron* **82,** 24-45.

Stephani F, Scheuer V, Eckrich T, Blum K, Wang W, Obermair GJ & Engel J. (2019). Deletion of the Ca(2+) Channel Subunit alpha(2)delta3 Differentially Affects Ca(v)2.1 and Ca(v)2.2 Currents in Cultured Spiral Ganglion Neurons Before and After the Onset of Hearing. *Front Cell Neurosci* **13,** 278.

Szabo Z, Obermair GJ, Cooper CB, Zamponi GW & Flucher BE. (2006). Role of the synprint site in presynaptic targeting of the calcium channel CaV2.2 in hippocampal neurons. *The European journal of neuroscience* **24,** 709-718.

Takahashi SX, Miriyala J & Colecraft HM. (2004). Membrane-associated guanylate kinase-like properties of beta-subunits required for modulation of voltage-dependent Ca2+ channels. *Proc Natl Acad Sci U S A* **101,** 7193-7198.

Tarabichi O, Correa T, Kul E, Phillips S, Darkazanly B, Young SM, Jr. & Hansen MR. (2023). Development and evaluation of helper dependent adenoviral vectors for inner ear gene delivery. *Hear Res* **435,** 108819.

Voigt A, Freund R, Heck J, Missler M, Obermair GJ, Thomas U & Heine M. (2016). Dynamic association of calcium channel subunits at the cellular membrane. *Neurophotonics* **3,** 041809.

Wang S, Stanika RI, Wang X, Hagen J, Kennedy MB, Obermair GJ, Colbran RJ & Lee A. (2017a). Densin-180 Controls the Trafficking and Signaling of L-Type Voltage-Gated Ca(v)1.2 Ca(2+) Channels at Excitatory Synapses. *J Neurosci* **37,** 4679-4691.

Wang S, Stanika RI, Wang X, Hagen J, Kennedy MB, Obermair GJ, Colbran RJ & Lee A. (2017b). Densin-180 Controls the Trafficking and Signaling of L-Type Voltage-Gated Cav1.2 Ca2+ Channels at Excitatory Synapses. *J Neurosci* **37,** 4679-4691.

Wei X, Neely A, Lacerda AE, Olcese R, Stefani E, Perez-Reyes E & Birnbaumer L. (1994). Modification of Ca2+ channel activity by deletions at the carboxyl terminus of the cardiac alpha 1 subunit. *The Journal of biological chemistry* **269,** 1635-1640.

Weiss N & Zamponi GW. (2017). Trafficking of neuronal calcium channels. *Neuronal Signal* **1,** NS20160003.

Wiser O, Cohen R & Atlas D. (2002). Ionic dependence of Ca2+ channel modulation by syntaxin 1A. *Proc Natl Acad Sci U S A* **99,** 3968-3973.

Wu LG, Westenbroek RE, Borst JG, Catterall WA & Sakmann B. (1999). Calcium channel types with distinct presynaptic localization couple differentially to transmitter release in single calyx-type synapses. *The Journal of neuroscience : the official journal of the Society for Neuroscience* **19,** 726-736.

Xie M, Li X, Han J, Vogt DL, Wittemann S, Mark MD & Herlitze S. (2007). Facilitation versus depression in cultured hippocampal neurons determined by targeting of Ca2+ channel Cavbeta4 versus Cavbeta2 subunits to synaptic terminals. *The Journal of cell biology* **178,** 489-502.

Yokoyama CT, Myers SJ, Fu J, Mockus SM, Scheuer T & Catterall WA. (2005). Mechanism of SNARE protein binding and regulation of Cav2 channels by phosphorylation of the synaptic protein interaction site. *Mol Cell Neurosci* **28,** 1-17.

Young SM, Jr. & Neher E. (2009). Synaptotagmin has an essential function in synaptic vesicle positioning for synchronous release in addition to its role as a calcium sensor. *Neuron* **63,** 482-496.

Young SM, Jr. & Veeraraghavan P. (2021). Presynaptic voltage-gated calcium channels in the auditory brainstem. *Mol Cell Neurosci* **112,** 103609.

Zhong H, Yokoyama CT, Scheuer T & Catterall WA. (1999). Reciprocal regulation of P/Q-type Ca2+ channels by SNAP-25, syntaxin and synaptotagmin. *Nat Neurosci* **2,** 939-941.

Additional information section

Conflict of Interest – the authors report no conflict of interest.

Author contributions: J.L. and P.V., carried out experiments and analyzed data. S.M.Y, Jr developed the mouse model S.M.Y, Jr planned the project and analyzed data. J.L. and S.M.Y, Jr. wrote the manuscript. All authors jointly revised the paper. All authors approved the final version of the manuscript, agree to be accountable for all aspects of the work in ensuring that questions related to the accuracy or integrity of any part of the work are appropriately investigated and resolved, all persons designated as authors qualify for authorship, and all those who qualify for authorship are listed.

Funding sources: This work was supported by the National Institutes of Deafness and Communication Disorders (R01 DC014093), the National Institute of Neurological Disorders and Stroke (R01 NS110742), and the National Center for Advancing Translational Sciences. R03TR004161-01 and the University of Iowa Distinguished Scholar Award. (S.M.Y., Jr) and the American Heart Association (Predoctoral fellowship 23PRE1019152) (J. L)

Acknowledgements: We thank members of the Young lab for their comments and critiques of the manuscript and project. We thank Hao Li for help with HdAd viral vector production. We thank Dr. Susan Stamnes and University of Iowa viral vector core, for help with HdAd vector production and tittering. We thank Dr. Phillip Ng for HdAd packing plasmids. We thank Dr. Chris Ahern and Miranda Schene for sharing HEK293T cells and HEK293T whole cell recording protocols. We thank Dr. Henry Colecraft for gifts of CMV $Ca_V\beta4$ plasmid.

1149

1150 .

Fig. 1

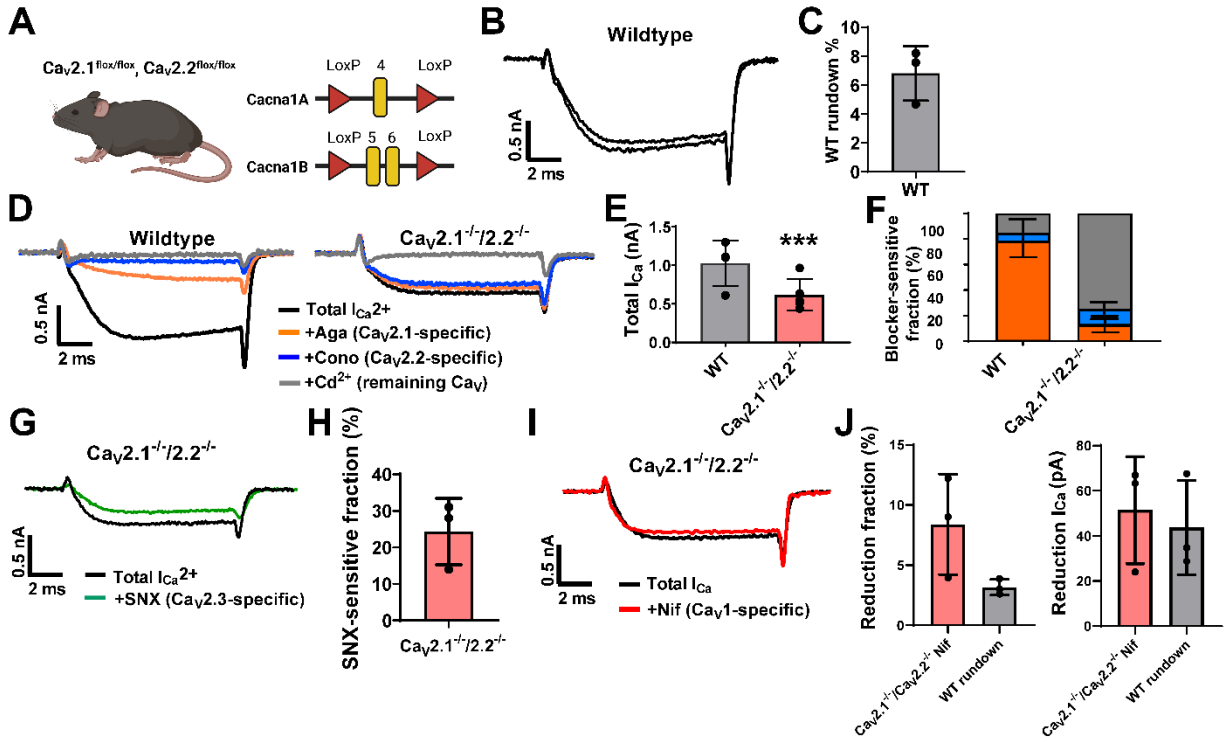

1151

1152

1153

Fig. 2

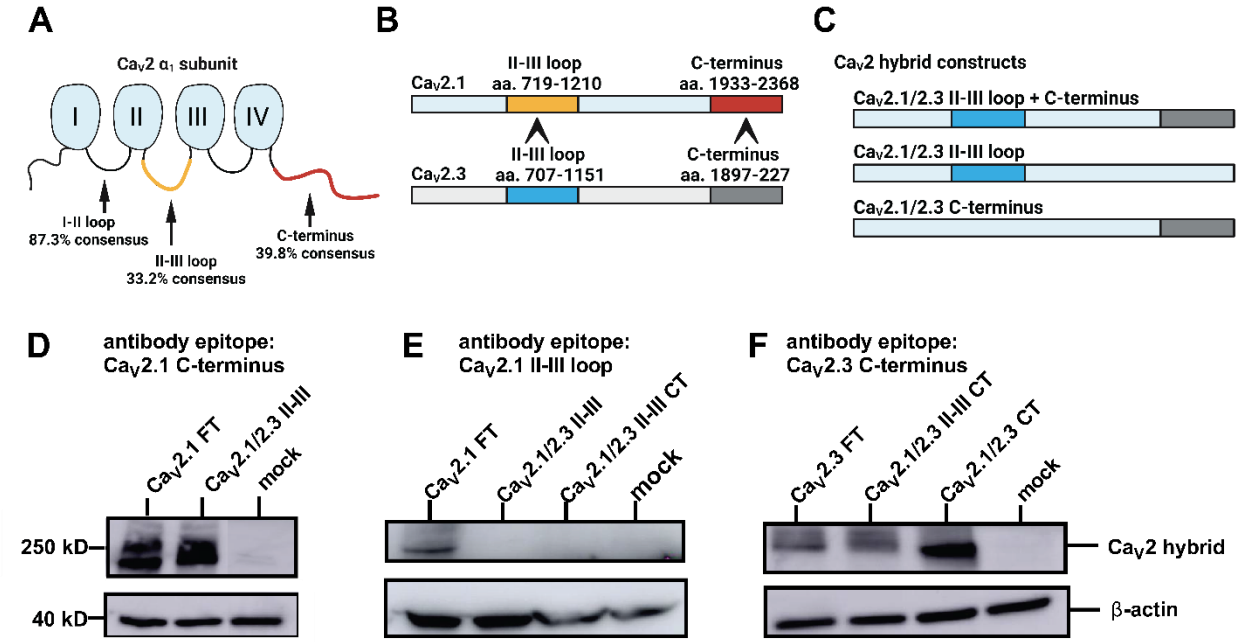

1154

1155

1156

1157

1158

Fig. 3

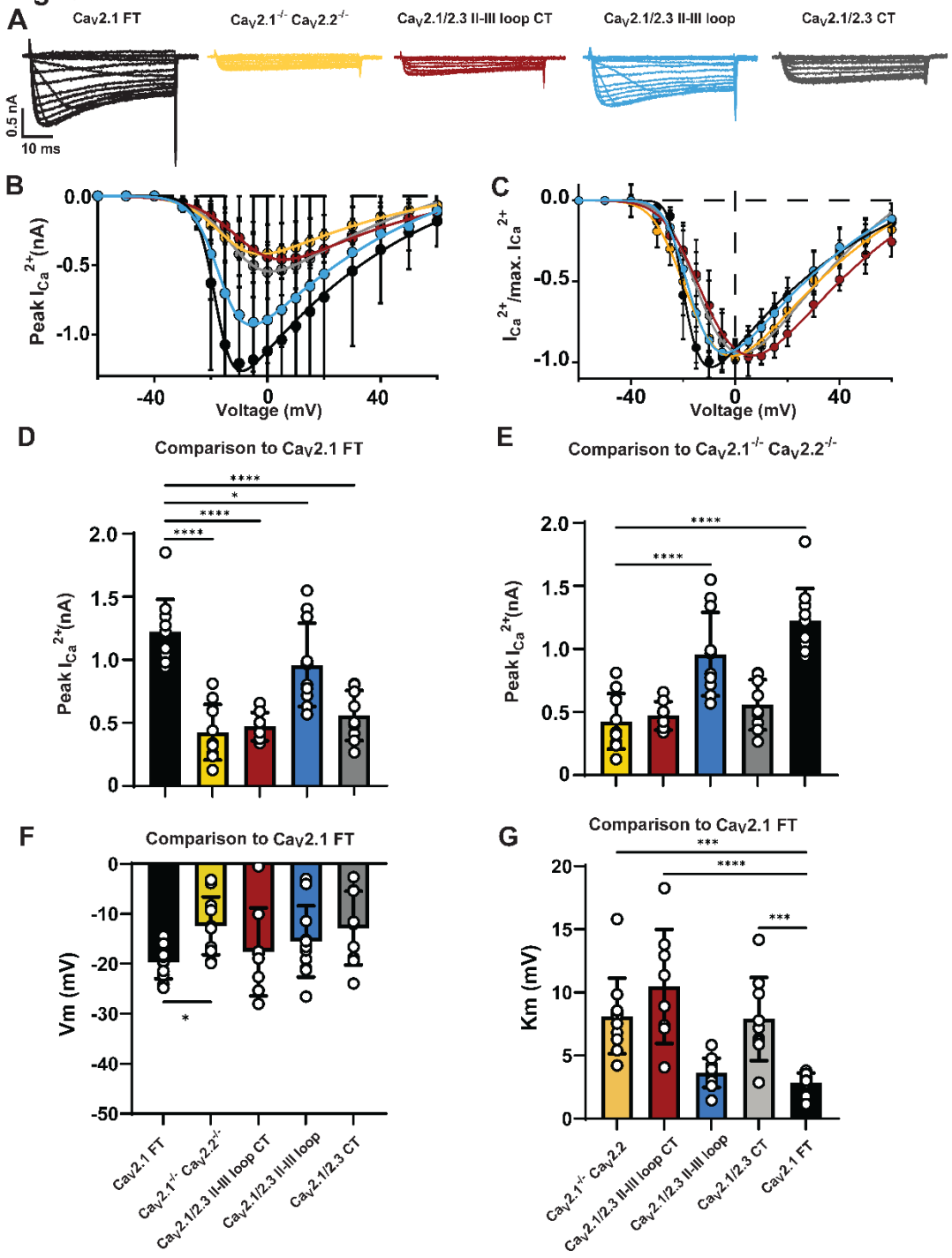

1159

1160

Fig. 4

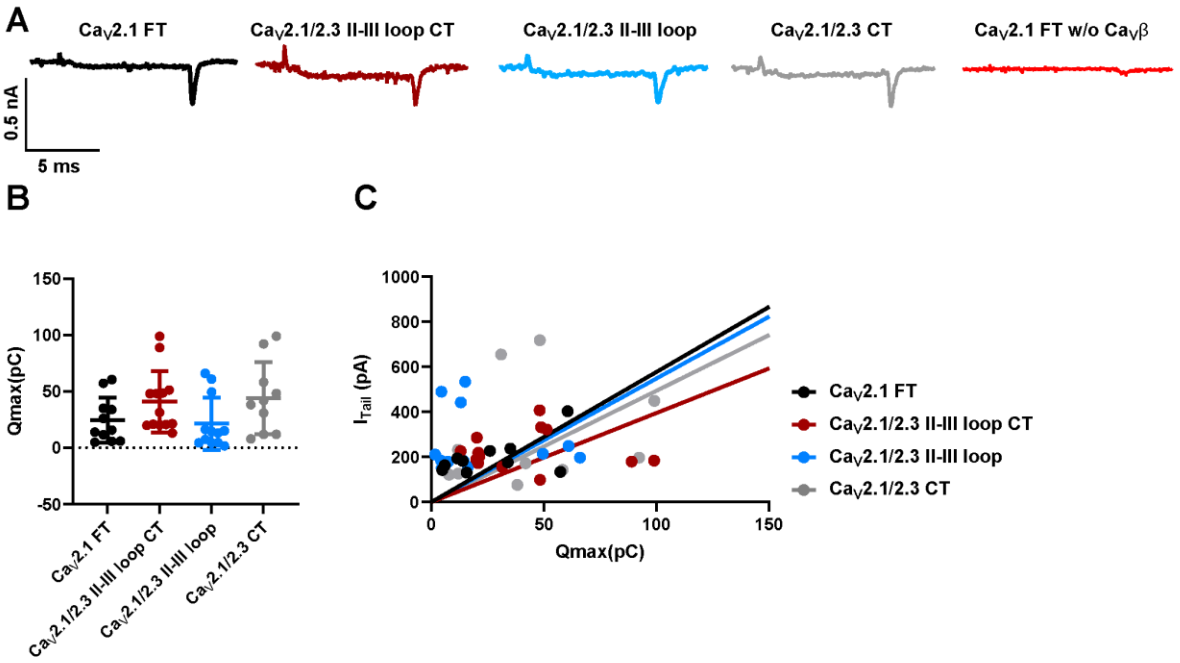
A
CaV2.1 FT
CaV2.1/2.3 II-III loop CT
CaV2.1/2.3 II-III loop
CaV2.1/2.3 CT
CaV2.1 FT w/o CaVβ
0.5 nA
5 ms
B
Qmax(pC)
150
100
50
0
-50
CaV2.1 FT
CaV2.1/2.3 II-III loop CT
CaV2.1/2.3 II-III loop
CaV2.1/2.3 CT
C
ITail (pA)
1000
800
600
400
200
0
0
50
100
150
Qmax(pC)
CaV2.1 FT
CaV2.1/2.3 II-III loop CT
CaV2.1/2.3 II-III loop
CaV2.1/2.3 CT

Fig. 5

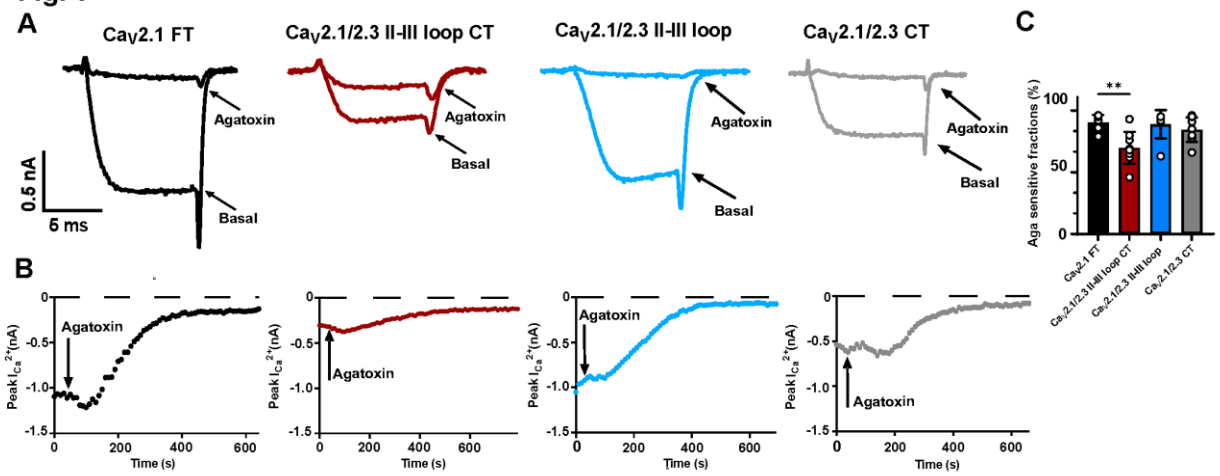
A
CaV2.1 FT
CaV2.1/2.3 II-III loop CT
CaV2.1/2.3 II-III loop
CaV2.1/2.3 CT
Agatoxin
Basal
0.5 nA
5 ms
B
Peak ICa 2+(nA)
Time (s)
C
Aga sensitive fractions (%)
**
CaV2.1 FT
CaV2.1/2.3 II-III loop CT
CaV2.1/2.3 II-III loop
CaV2.1/2.3 CT

1175

Fig. 6

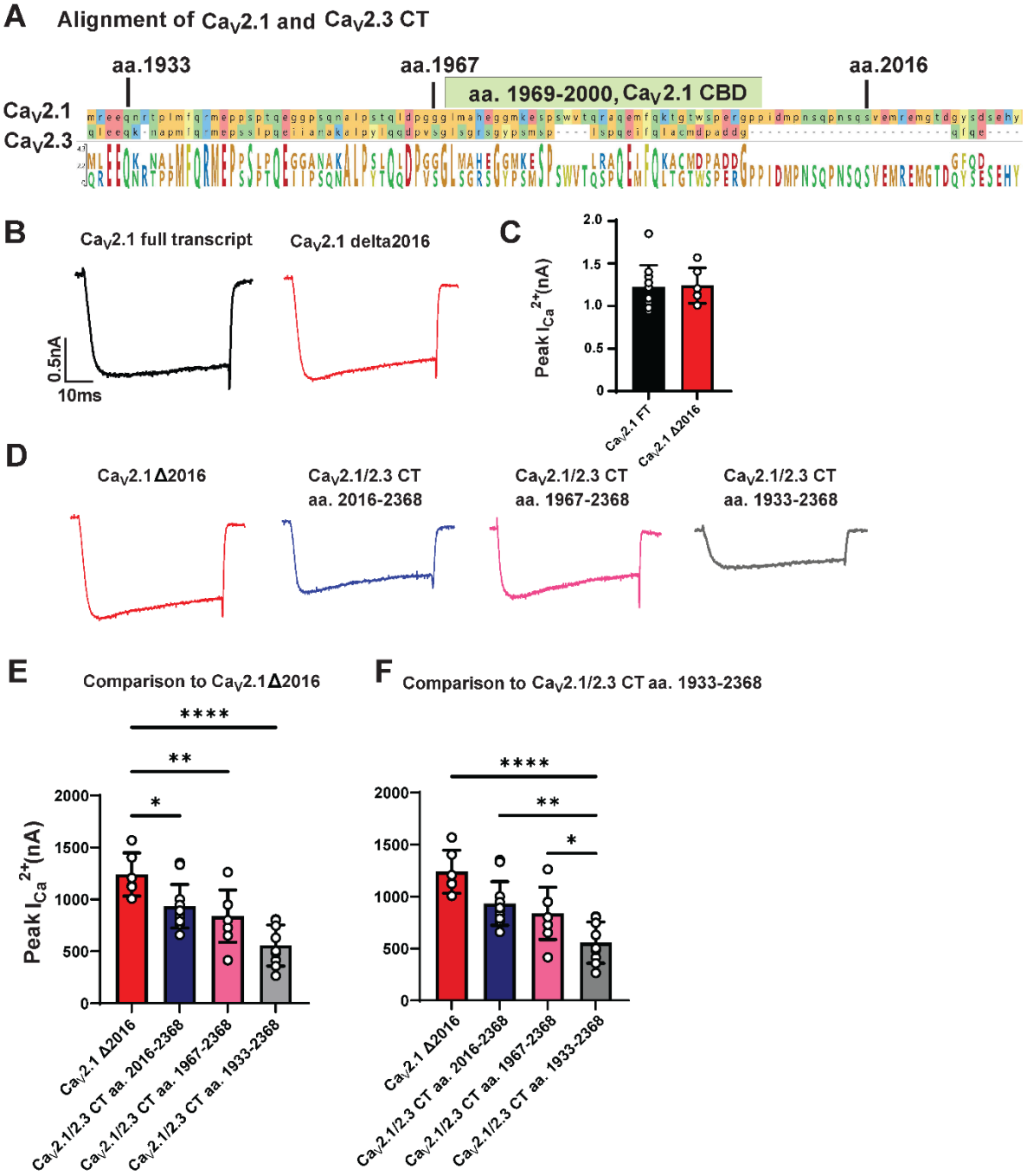

1176

1177

1178

1179

1180

1181

1182

Fig. 7

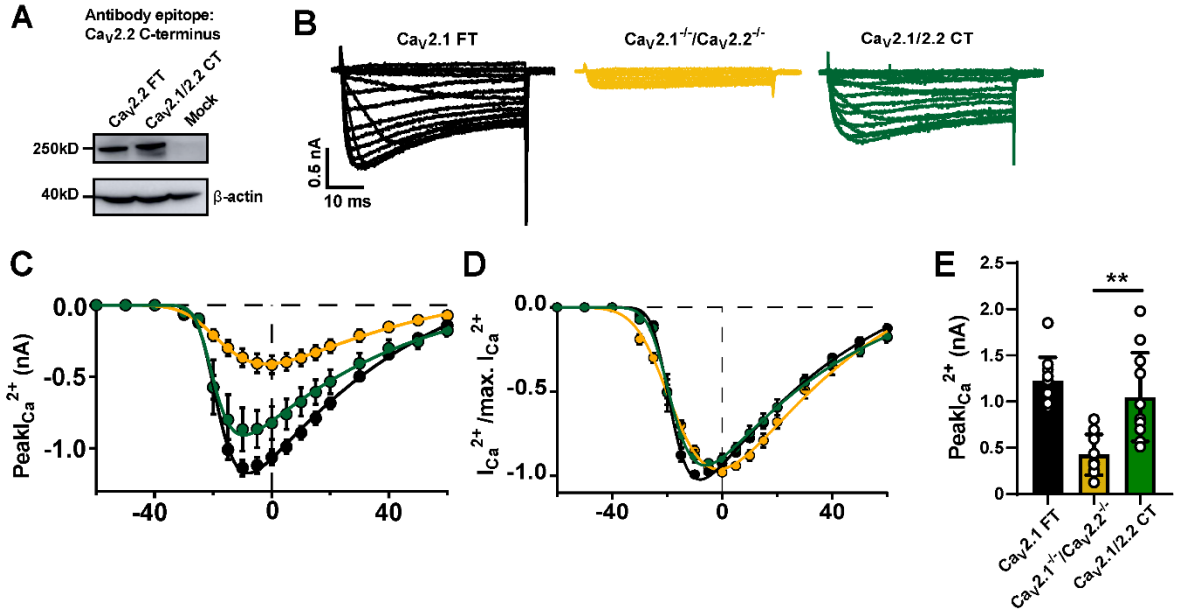

1183

1184

1185

Fig. 8

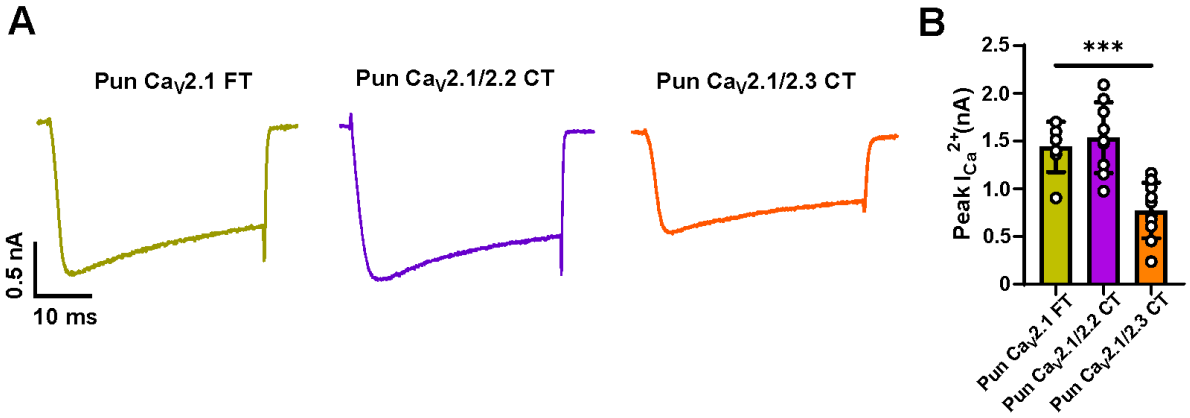

1186